Cell Reports

Article

The glycolysis/HIF-1α axis defines the inflammatory role of IL-4-primed macrophages

Graphical abstract

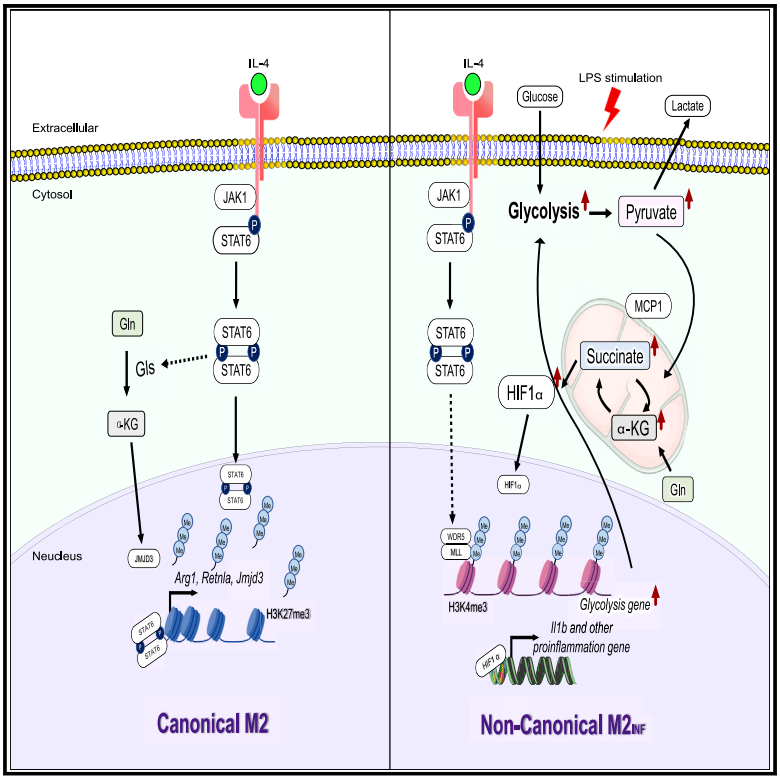

Highlights

- Non-canonical $M2_{INF}$ macrophages show proinflammatory phenotype upon microbial stimulation
- Glycolysis supports Hif-1α stabilization in $M2_{INF}$ macrophages
- Wdr5-dependent H3K4me3 modification is integral to $M2_{INF}$ macrophages
- Acute IL-4 exposure elicits $M2_{INF}$ macrophages *in vivo* and augments antibacterial response

Authors

Buyun Dang, Qingxiang Gao, Lishan Zhang, ..., Stanley Ching-Cheng Huang, Ping-Chih Ho, Shih-Chin Cheng

Correspondence

jamescheng@xmu.edu.cn

In brief

Dang et al. reveal that IL-4 preconditioning generates potent M2 inflammatory macrophages with enhanced proinflammatory potential. Metabolic reprogramming, Hif-1α stabilization, and Wdr5-dependent H3K4me3 modification are factors shaping this phenotype. Acute IL-4 treatment bolsters resistance to bacterial infection, broadening our understanding of IL-4-mediated effects and transforming approaches for Th2-associated inflammatory diseases.

Dang et al., 2023, Cell Reports *42*, 112471
May 30, 2023
https://doi.org/10.1016/j.celrep.2023.112471

CellPress

Cell Reports

CellPress
OPEN ACCESS

Article

The glycolysis/HIF-1α axis defines the inflammatory role of IL-4-primed macrophages

Buyun Dang,[1,2,7] Qingxiang Gao,[1,7] Lishan Zhang,[1,7] Jia Zhang,[1,7] Hanyi Cai,[1] Yanhui Zhu,[1] Qiumei Zhong,[1] Junqiao Liu,[1] Yujia Niu,[1] Kairui Mao,[1] Nengming Xiao,[1] Wen-Hsien Liu,[1] Shu-hai Lin,[1] Jialiang Huang,[1] Stanley Ching-Cheng Huang,[3] Ping-Chih Ho,[4,5] and Shih-Chin Cheng[1,2,6,8,*]

[1]State Key Laboratory of Cellular Stress Biology, School of Life Science, Faculty of Medicine and Life Sciences, Xiamen University, Xiamen 361102, China

[2]Department of Gastroenterology, The National Key Clinical Specialty, Zhongshan Hospital of Xiamen University, School of Medicine, Xiamen University, Xiamen, Fujian 361004, China

[3]Department of Pathology, Case Western Reserve University School of Medicine, Cleveland, OH, USA

[4]Ludwig Institute for Cancer Research, University of Lausanne, Epalinges, Vaud, Switzerland

[5]Department of Oncology, University of Lausanne, Epalinges, Switzerland

[6]Department of Digestive Disease, School of Medicine, Xiamen University, Xiamen, Fujian 361004, China

[7]These authors contributed equally

[8]Lead contact

*Correspondence: jamescheng@xmu.edu.cn

https://doi.org/10.1016/j.celrep.2023.112471

SUMMARY

T helper type 2 (Th2) cytokine-activated M2 macrophages contribute to inflammation resolution and wound healing. This study shows that IL-4-primed macrophages exhibit a stronger response to lipopolysaccharide stimulation while maintaining M2 signature gene expression. Metabolic divergence between canonical M2 and non-canonical proinflammatory-prone M2 ($M2_{INF}$) macrophages occurs after the IL-4Rα/Stat6 axis. Glycolysis supports Hif-1α stabilization and proinflammatory phenotype of $M2_{INF}$ macrophages. Inhibiting glycolysis blunts Hif-1α accumulation and $M2_{INF}$ phenotype. Wdr5-dependent H3K4me3 mediates the long-lasting effect of IL-4, with Wdr5 knockdown inhibiting $M2_{INF}$ macrophages. Our results also show that the induction of $M2_{INF}$ macrophages by IL-4 intraperitoneal injection and transferring of $M2_{INF}$ macrophages confer a survival advantage against bacterial infection *in vivo*. In conclusion, our findings highlight the previously neglected non-canonical role of $M2_{INF}$ macrophages and broaden our understanding of IL-4-mediated physiological changes. These results have immediate implications for how Th2-skewed infections could redirect disease progression in response to pathogen infection.

INTRODUCTION

IL-4 is a prototypic immunomodulatory cytokine with diverse functions, such as regulation of immunoglobulin isotype switch,[1,2] induction of MHC II[3] and CD23 expression,[4] regulation of hematopoiesis,[5] etc. Among its multiple functions, the canonical role of IL-4 is to induce alternative macrophage activation, also known as M2.[6,7] M2 macrophages are considered anti-inflammatory, releasing factors like arginase-1, IL-10, TGF-β, and other anti-inflammatory cytokines. This helps resolve inflammation, aids in wound healing, and is linked to tumor development and progression in the context of tumor-associated macrophages (TAMs). When IL-4 binds to the IL-4 receptor alpha subunit (IL-4Rα), it triggers phosphorylation of STAT6, which then forms dimers and moves into the nucleus to activate transcription of M2 signature genes.

The concept of M1 and M2 macrophage polarization is well established *in vitro*, but *in vivo*, macrophages in a pathophysiological or homeostatic state often express a mixture of M1 and M2 signature markers.[7,8] Thus, a revised view of macrophage activation or differentiation is a spectrum or continuum concept, emphasizing the plastic nature of macrophage activation and differentiation. For instance, when encountering invading pathogens, macrophages are quickly activated through recognition of pattern recognition receptors and pathogen-associated molecular patterns (PAMPs) and differentiate into proinflammatory M1-like macrophages during the acute inflammatory phase. However, the inflammatory response must be resolved when the host immune system clears the invaders, leading to a switch from proinflammatory M1 to anti-inflammatory M2 macrophages over time to suppress inflammation and facilitate wound healing at the resolution phase.

The repolarization of macrophage phenotype is considered a potential therapeutic approach in various diseases and pathological settings. For instance, shifting TAMs from an M2 to an M1 phenotype may be beneficial in fighting cancer.[9] Reprogramming

proinflammatory M1 toward M2 macrophages might be favorable in ameliorating proinflammatory diseases such as obesity[10] and atherosclerosis.[11] Surprisingly, we found that even though they are IL-4 primed, macrophages expressing typical M2 signature genes such as *Arg1* and *Retnla* at the basal state have a robust proinflammatory potential upon lipopolysaccharide (LPS) stimulation, compared with naive and M1 macrophages. This suggests that the long-held view of IL-4-induced M2 macrophages may need to be reconsidered, as it only applies in the context of M2 macrophages not encountering subsequent proinflammatory stimuli, such as LPS or other PAMPs. Here, we uncovered a non-canonical proinflammatory-prone feature of IL-4 and delineated that IL-4-induced canonical M2 and non-canonical proinflammatory-prone M2 ($M2_{INF}$) macrophages diverge metabolically after the common IL-4Rα/Jak1/Stat6 axis. Elevated glycolysis and Hif-1α are defining factors for the IL-4 non-canonical $M2_{INF}$ macrophage arm, while the Gln/α-KG axis is responsible for the canonical M2 macrophage arm. We also show that IL-4 induces non-canonical $M2_{INF}$ macrophages *in vivo* and renders mice more resistant to bacterial infections. Therefore, this previously neglected non-canonical aspect of IL-4 biology in macrophages has the potential to broaden our understanding of the unresolved association between type 2 immunity-bias diseases, such as asthma and allergy, and other inflammatory diseases, such as sepsis[12] and obesity.[13,14]

RESULTS

IL-4 induces non-canonical proinflammatory $M2_{INF}$ macrophages

Mouse bone-marrow-derived macrophage (BMDM) polarization and repolarization capacity were examined *in vitro* by stimulation with LPS/IFNγ or IL-4 (Figure S1A). Surprisingly, M2 macrophages exhibited a higher level of M1 gene (Figure S1B) and secreted more TNF-α, IL-6, and nitric oxide (NO) upon LPS/IFNγ stimulation (Figure S1C). However, in accordance with previous reports,[15,16] M1 macrophages could not repolarize to M2 macrophages, as demonstrated by the expression levels of *Arg1* and *Retnla* (Figure S1D). Therefore, we speculate that, on the one hand, the canonical function of IL-4 is to induce M2 macrophage differentiation. However, on the other hand, IL-4 induces a non-canonical effect to "inflame" $M2_{INF}$ macrophages upon subsequent stimulation. To examine the non-canonical role of IL-4, we pretreated BMDMs with IL-4 for 24 h and rested them for an additional 24 h in a fresh medium before subsequent LPS stimulation (Figure 1A). As a result, *Il6*, *Il1β*, and *Il12a* gene expression (Figure 1B) and IL-6 and NO secretion, as well as intracellular pro-IL-1β level, were upregulated (Figures 1C and S1E). These findings suggest that IL-4 treatment sensitizes macrophages to become more proinflammatory upon subsequent stimulation. Furthermore, we observed that $M2_{INF}$ macrophages displayed a broad-spectrum proinflammatory effect, as evidenced by increased production of proinflammatory cytokines IL-6 and NO in response to stimulation with both Pam3Cys (a TLR2 agonist) and heat-killed *Candida albicans* (Figure S1F).

We also investigated the impact of the duration of IL-4 stimulation on macrophage phenotype (Figure 1D). Macrophages that received persistent IL-4 signaling for 48 h (p-$M2_{INF}$) produced higher IL-6 and NO than the 24-h exposure group ($M2_{INF}$) (Figure 1E), albeit maintaining the high expression of M2 signature genes *Retnla* and *Arg1* (Figure 1F). This suggests that persistent IL-4 stimulation induces a heightened proinflammatory effect while retaining M2 signature gene expression. In addition, when IL-4-treated BMDMs were simultaneously stimulated with LPS and IL-4, there was a further boost in *Il6* expression, while *Il10* expression was suppressed (Figure S1G). These findings provide further evidence of the non-canonical role of IL-4 in modulating macrophage phenotype and function.

Intrigued by the fact that IL-4 induces a more robust proinflammatory response in macrophages upon stimulation, we wondered whether other type 2 cytokines have a similar effect. We found that IL-13, but not IL-5, upregulated proinflammatory phenotype in BMDMs (Figures 1G and S1H), suggesting the signaling transduction via IL-4Rα might be crucial in the non-canonical function observed. Surprisingly, the type 1 cytokine IFNγ failed to induce proinflammatory phenotype. Instead, pretreatment with IFNγ increased *Il10* expression upon subsequent LPS stimulation (Figure S1I). When stimulation was performed with both IFNγ and IL-4, a response similar to that of IL-4 single stimulation was observed (Figures 1G and S1H), indicating the presence of IL-4 plays a dominant role in the elicitation of $M2_{INF}$ macrophages. Together, these results suggest that the non-canonical $M2_{INF}$ macrophages may be triggered by both acute and persistent exposure to IL-4 during type 2 responses where IL-4 and IL-13 levels are elevated.

IL-4 induces $M2_{INF}$ macrophages in an IL-4Rα/Stat6-dependent and Gln/α-KG/Jmjd3 axis-independent manner

IL-4Rα is the common receptor for IL-4 and IL-13 signaling. As expected, IL-4 failed to induce M2 macrophage polarization in BMDMs derived from *IL-4Rα* MKO (*IL-4Ra$^{f/f}$ Lyz2-cre* myeloid-specific knockout) (Figure S2A). Furthermore, the induction of $M2_{INF}$ macrophages was also impaired in *IL-4Rα* MKO (Figure 2A). Stat6-phosphorylation downstream of IL-4Rα is critical for IL-4-induced M2 polarization. Knockdown of Stat6 by shRNA impaired IL-4 mediated M2 gene *Arg1* (Figure S2B). Meanwhile, IL-4-induced $M2_{INF}$ macrophages were also inhibited as expression of *IL-6* and *IL-1β* was reduced (Figure 2B), suggesting that Stat6 is indispensable for IL-4-induced canonical M2 and non-canonical $M2_{INF}$ macrophages.

As glutamine/α-ketoglutarate/Jmjd3 axis is critical for IL-4-induced M2 macrophage polarization,[17,18] we further investigated whether this axis is responsible for the non-canonical $M2_{INF}$ macrophages. In line with the previous report, M2 signature genes such as *Arg1* and *Retnla* were downregulated in glutamine-free conditions (Figure 2C), while the proinflammatory genes (Figure 2D), protein, and NO expression (Figure 2E) were not influenced. The inhibition of glutaminolysis or Jmjd3 activity by BPTES or GSK-J4 impaired the expression of the M2 signature (Figures S2C and S2D). However, treating with BPTES and GSK-J4 also inhibited the proinflammatory response even in the absence of IL-4, which prevented us from assessing their role in IL-4-induced non-canonical effects (Figures S2E and S2F). Therefore, we speculated that acute inhibition with BPTES and GSK-J4 might have a pleiotropic effect on inhibiting inflammatory genes. To address this issue,

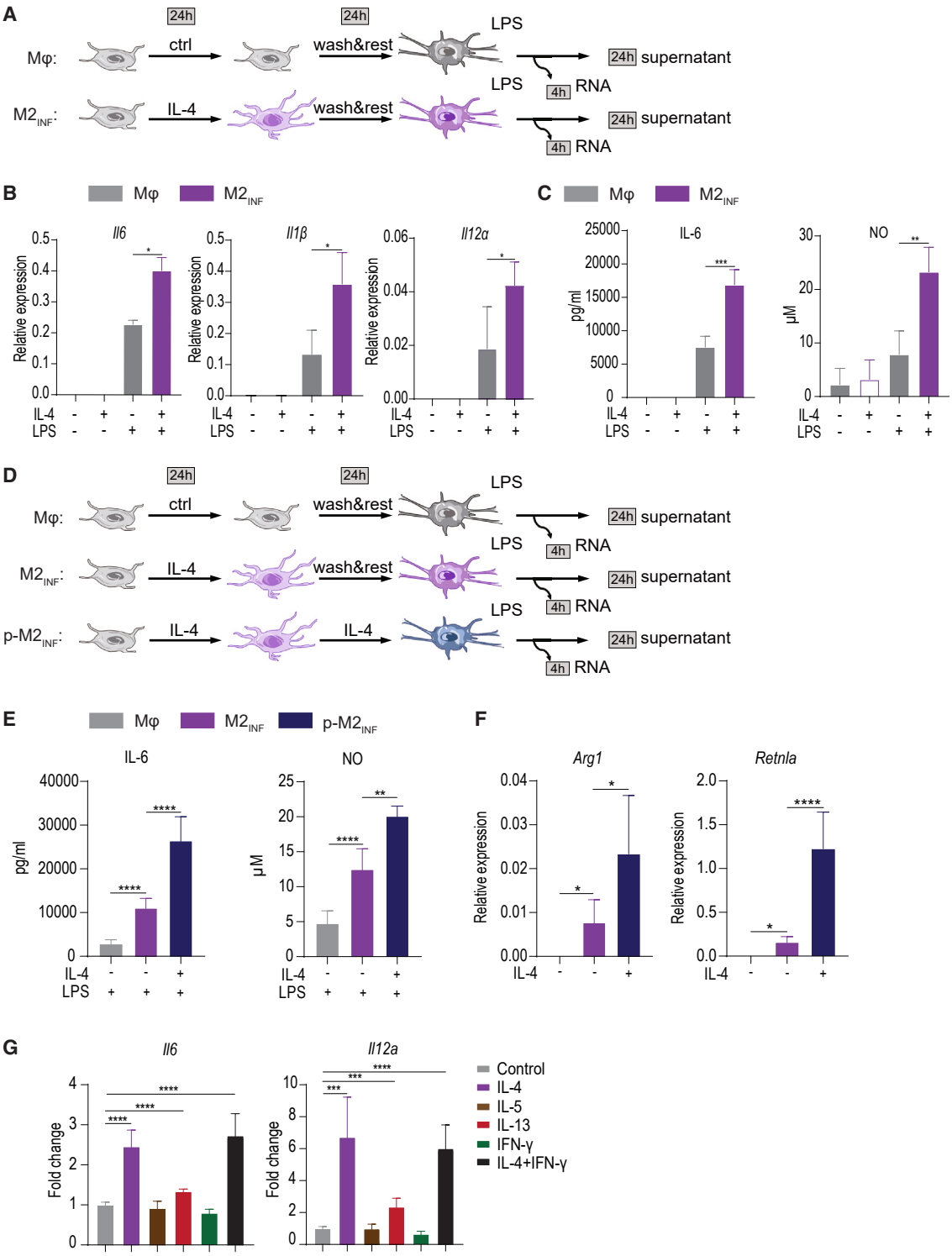

Figure 1. IL-4 induced non-canonical $M2_{INF}$ macrophages

(A) Schematic of the experimental setup.

(B) IL-4-stimulated BMDMs were analyzed with LPS stimulation for 4 h, and mRNA was collected for qPCR analysis.

(C) IL-6 and NO production were measured 24 h after LPS stimulation.

(D) Experimental setup for prolonged IL-4 stimulation.

(E and F) IL-6 and NO production (E) and M2 gene expression (F) were measured.

(G) BMDMs pretreated with cytokines were analyzed for mRNA expression after LPS stimulation. *$p < 0.05$, **$p < 0.01$, ***$p < 0.001$, ****$p < 0.0001$, unpaired, two-tailed Student's t test. Data represent three independent experiments with three to four samples per group (mean ± SD).

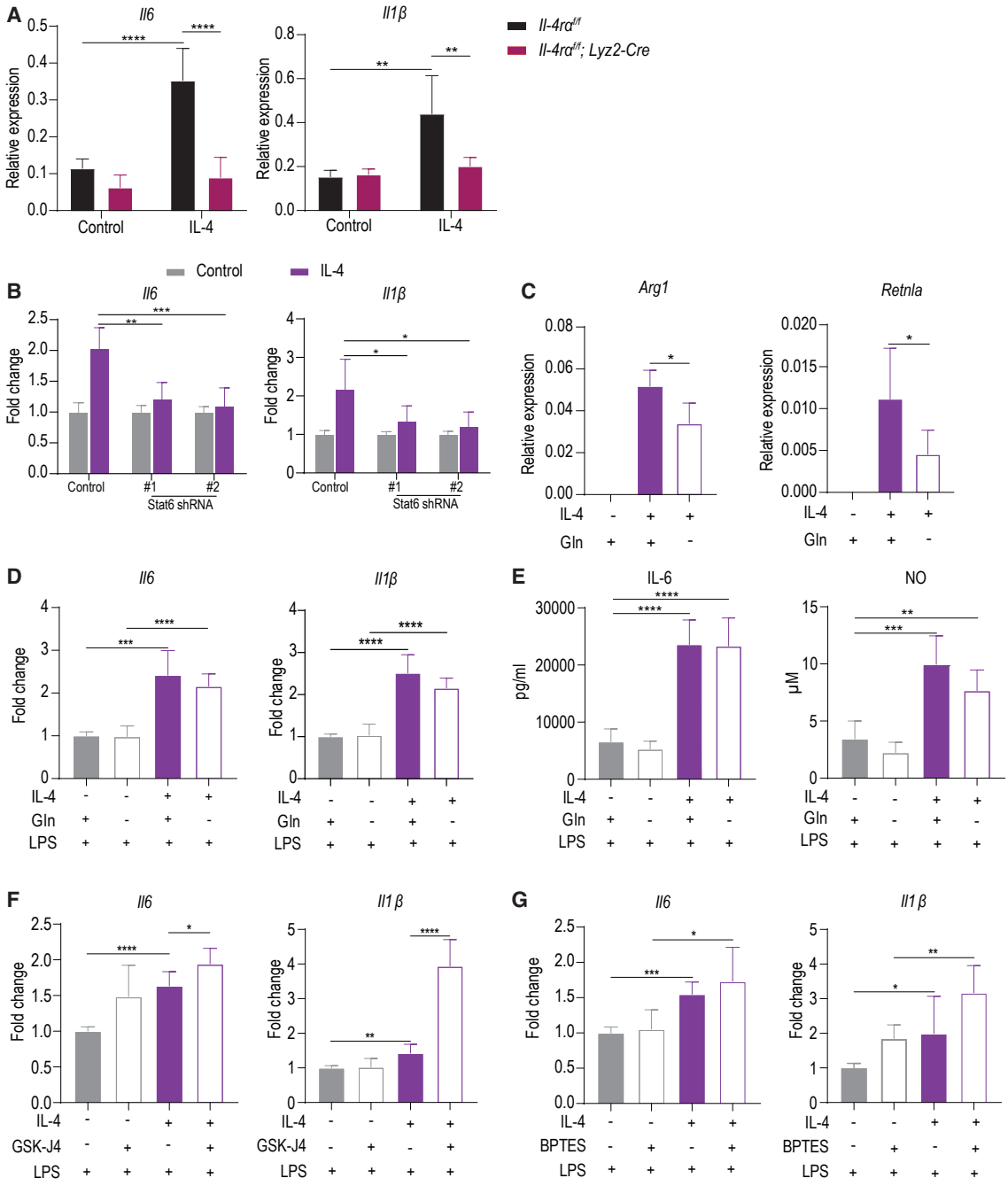

Figure 2. IL-4 induced $M2_{INF}$ macrophages in a Stat6-dependent and Gln/α-KG/Jmjd3 axis-independent manner

(A) qPCR mRNA expression of cytokine genes in wild-type littermate and IL-4Rα MKO BMDMs stimulated with LPS at 24 h post IL-4 stimulation.

(B–D, F, and G) qPCR mRNA expression of cytokine genes (B, D, F, and G) and M2 marker genes (C) in BMDMs stimulated with IL-4 or LPS at 24 h post IL-4 stimulation under various culture conditions as indicated.

(E) Corresponding IL-6 and NO production were measured from the supernatant harvested 24 h post LPS stimulation. *$p < 0.05$, **$p < 0.01$, ***$p < 0.001$, ****$p < 0.0001$, unpaired, two-tailed Student's t test. Data are representative of three independent experiments with three to four samples per group (mean ± SD).

IL-4-treated BMDMs were rested for an additional 5 days before restimulation, allowing the acute inhibition effects of BPTES and GSK-J4 to wash away. Nevertheless, both inhibitors did not affect the non-canonical IL-4-induced proinflammatory cytokines, as shown in Figures 2F and 2G. Additionally, the cell viability of both control and $M2_{INF}$ macrophages was comparable 6 days before LPS restimulation (Figure S2G). Our results indicate that the IL4/Stat6 axis is essential for canonical M2 and non-canonical $M2_{INF}$ polarization. In contrast, while the Gln/α-KG/jmjd3 axis is critical for M2 polarization, it appears dispensable for $M2_{INF}$ polarization.

Transcriptomics analysis reveals the inflammatory-prone feature of $M2_{INF}$ macrophages

We further performed RNA-seq analysis to acquire a panoramic view of the transcriptomic profile induced by IL-4. There were 610 differential expression genes between the control and IL-4-treated groups, including classic M2 genes *Retnla*, *Chil3,* and *Mgl2* in the top regulated genes, shown in the volcano plot (Figure 3A). In line with the previous report,[19] oxidative phosphorylation was among the topmost enriched metabolic pathway in upregulated genes by KEGG (Kyoto Encyclopedia of Genes and Genomes) analysis (Figure 3B). As metabolic reprogramming plays a pivotal role in macrophage activation, we performed the gene set enrichment analysis (GSEA) with particular focus on the metabolic pathways to find out which functional phenotypes were enriched in IL-4 group and associated with its non-canonical feature. Pathways such as oxidative phosphorylation, glucose catabolic process, and specifically glycolysis were significantly enriched in IL-4-treated macrophages (Figure 3C).

We further assessed the gene expression profile focusing on LPS-upregulated genes (Figure S3A). LPS upregulated classic pathways, including TNF, NF-κB, and cytokine/chemokine signaling pathways (Figure S3B). We subdivided the differential expressed genes into three clusters: C1 (upregulated), C2 (unaffected), and C3 (downregulated) by comparing the expression level between control and IL-4-treated macrophages, and performed KEGG pathways enrichment analysis for each cluster (Figures 3D and S3C). Proinflammatory genes, such as *Il6*, *Il12a*, and *Il1β*, were encompassed in cluster C1 in line with the qPCR results (Figure 1B). The Gene Ontology (GO) enrichment analysis of the C1 also revealed the enrichment of TNF, NF-κB, and Toll-like receptor signaling pathways (Figure 3E), supporting the idea of the non-canonical feature of IL-4 in promoting proinflammatory response.

$M2_{INF}$ macrophages are more energetic and switch toward glycolysis upon LPS stimulation

Metabolic rewiring from oxidative phosphorylation toward glycolysis is essential for mounting efficient proinflammatory responses in macrophages.[20] To investigate the cellular metabolic profile of IL-4-treated macrophages, we analyzed the upregulation of glycolysis using RNA-seq analysis (Figure 3C). We observed a significant increase in lactate production in IL-4-treated macrophages upon LPS stimulation (Figure 4A). Additionally, we found an increase in essential glycolysis proteins such as Hk3, Pfkfb3, enolase1, aldolase A, and Glut1, the main glucose transporter (Figure 4B). These results indicate that a shift toward glycolysis metabolically underlines the heightened proinflammatory feature of $M2_{INF}$ macrophages.

We further assessed the effect of IL-4 on the energetic status of macrophages. In line with the increased lactate secretion, IL-4-treated macrophages upregulated glycolysis both at basal respiration and upon LPS stimulation and have a higher glycolytic capacity (Figure 4C). Basal respiration, ATP production, and maximal respiration capacity also increased by acute IL-4 treatment (Figure 4D). Given that the proinflammatory effect of $M2_{INF}$ macrophages lasts for at least 6 days post initial IL-4 stimulation (as illustrated in Figure 2F), we sought to investigate whether the metabolic profile of $M2_{INF}$ macrophages could persist for a longer duration. We found that similar to acute $M2_{INF}$ macrophages at 24 h, $M2_{INF}$ macrophages remained more committed to glycolysis and oxidative phosphorylation (OXPHOS) at day 6 (Figures S4A and S4B). Furthermore, our findings reveal that the elevated proinflammatory response and metabolic rewiring observed in $M2_{INF}$ macrophages are comparable to the trained immunity induced by β-glucan.[21] Collectively, these observations suggest that IL-4 may act as another trained immunity inducer. Overall, our results indicate that IL-4-treated macrophages are more energetically active at basal respiration and upon stimulation, as shown in Figures 4E and S4C.

We further performed stable isotope tracing in IL-4-stimulated macrophages with the tracer [U-$^{13}C_6$]-glucose. In agreement with the Seahorse results (Figure 4C), ^{13}C-labeled glycolytic intermediates were significantly increased in IL-4-stimulated macrophages (Figure 4F). Furthermore, the proportion of ^{13}C-labeled TCA cycle intermediates, such as citrate, α-ketoglutarate, succinate, and fumarate, was also primarily upregulated in IL-4-stimulated macrophages (Figure S4D), implying higher OXPHOS capacity, which is in line with the oxygen consumption rate (OCR) result (Figure 4D). Together, our metabolic analysis reveals that IL-4-treated macrophages, on the one hand, have upregulated OXPHOS capacity, which is the metabolic feature of M2 macrophages. On the other hand, the elevated glycolysis at both basal and activation states might be critical for the proinflammatory $M2_{INF}$ macrophages.

Glycolysis-mediated Hif-1α stabilization is critical for $M2_{INF}$ macrophages

Previous studies have shown that stabilization of hypoxia-inducible factor 1 alpha (Hif-1α) can prolong interleukin-1 beta (IL-1β) expression by promoting succinate accumulation.[22] In order to assess the impact of the glycolysis/Hif-1α axis on IL-4-treated macrophages, we employed a glycolytic inhibitor, 2-deoxyglucose (2-DG). The accumulation of Hif-1α and upregulation of pro-IL-1β and IL-6 were inhibited by 2-DG (Figures 5A and 5B). Similarly, the heightened Hif-1α accumulation and pro-IL-1β and IL-6 levels were blocked when IL-4-treated macrophages were cultured in a glucose-free medium (Figures 5C and 5D) or galactose-replacing medium (Figures 5E and 5F). Since the intracellular succinate level was upregulated in IL-4-treated macrophages (Figure 5G), we further examined the causal relationship between upregulated glycolysis and accumulated succinate level by blocking with a mitochondrial pyruvate carrier inhibitor UK5099. The Hif-1α and pro-IL-1β levels were also impaired by UK5099 (Figures 5H and 5I), suggesting mitochondrial pyruvate influx is crucial for the proinflammatory phenotype for $M2_{INF}$ macrophages. In addition, the enhanced accumulation of succinate by LPS stimulation blocked Jmjd3/α-KG-dependent M2 differentiation in $M2_{INF}$ macrophages (Figure S5).

We further assessed whether Hif-1α is also involved in IL-4-induced M2 differentiation in myeloid-specific *Hif-1α* MKO (*Hif-1α f/f Lyz2-cre* myeloid-specific knockout) BMDMs. Our results suggested that IL-4-induced M2 genes *Arg1* and *Retnla* expression were not influenced in *Hif-1α* MKO BMDMs (Figure 5J), while IL-4-induced non-canonical augmentation of *IL-1β* expression was impaired (Figure 5K). These results suggest that the glycolysis/Hif-1α axis is critical for IL-4-induced $M2_{INF}$ macrophages.

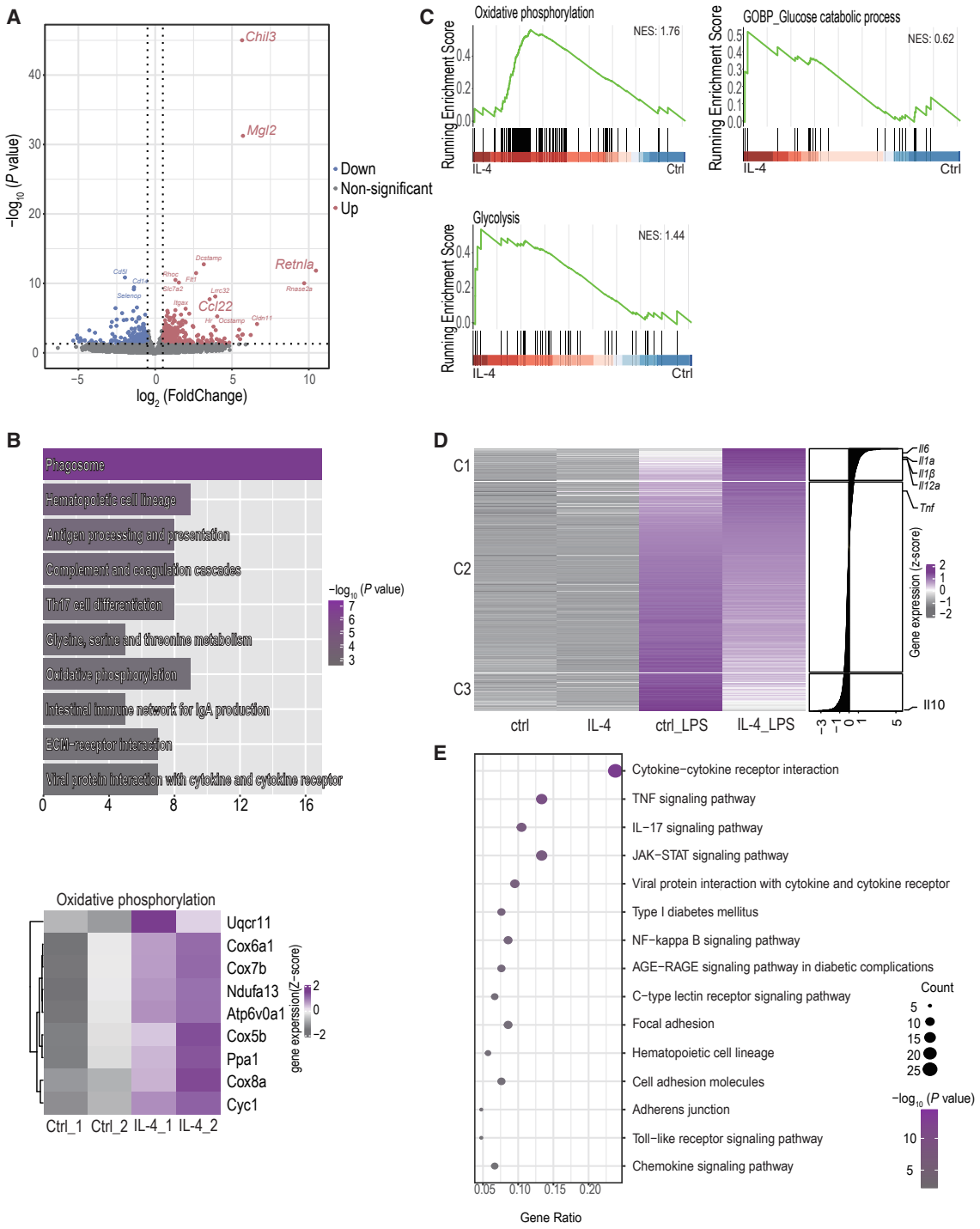

Figure 3. The transcriptomic profile of $M2_{INF}$ macrophages

(A) Volcano plot of differentially expressed genes between control and IL-4-treated BMDMs.

(B) Top 10 enriched pathways by KEGG analysis of upregulated genes in IL-4-treated BMDMs.

(C) Enrichment of oxidative phosphorylation, glucose catabolic process, and glycolysis in IL-4-treated macrophages shown by GSEA.

(D) Rank-normalized expression levels of LPS upregulated genes in control and IL-4-treated BMDMs divided into three clusters: C1 (Log2FC $\geq$ 0.5), C2 (0.5 $\geq$ Log2FC $\geq$ −0.5), and C3 (Log2FC $\leq$ −0.5).

(E) GO analysis of genes in the C1 cluster.

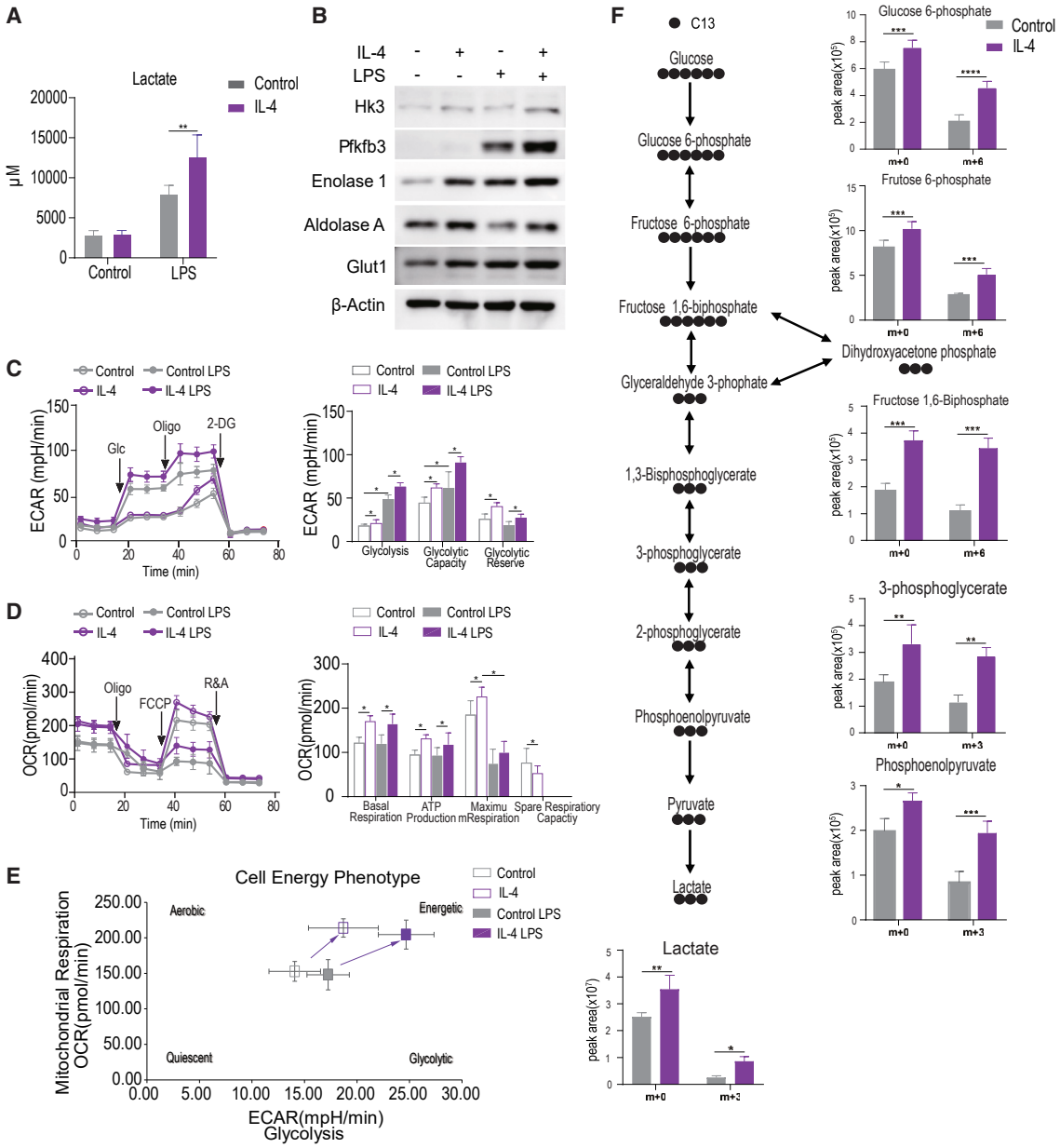

Figure 4. Metabolic characterization of $M2_{INF}$ macrophages

(A) Lactate concentration in supernatants from $M2_{INF}$ cells stimulated with LPS for 24 h.

(B) Western blot analysis of key glycolytic enzymes and glucose transporter Glut1 in control and $M2_{INF}$ macrophages stimulated with LPS for 3 h.

(C and D) Seahorse analysis of (C) extracellular acidification rate (ECAR) and glycolysis capacity and (D) OCR and mitochondrial respiration capacity in control and $M2_{INF}$ cells under basal conditions or after 3 h of LPS stimulation from two independent experiments.

(E) Energy profiles of BMDMs from control and $M2_{INF}$ cells at basal and LPS-stimulated states.

(F) Representative metabolites from $^{13}C6$-glucose in the glycolysis pathway determined by liquid chromatography-mass spectrometry/mass spectrometry (LC-MS/MS). *$p < 0.05$, **$p < 0.01$, ***$p < 0.001$, ****$p < 0.0001$, unpaired, two-tailed Student's t test. Data are representative of two independent experiments with two samples per group (mean ± SD).

Epigenetic determination of $M2_{INF}$ macrophages

Metabolic rewiring and epigenetic modification have been closely associated with macrophage differentiation status. Therefore, we performed assay for transposase-accessible chromatin with sequencing (ATAC-seq) to compare the chromatin accessibility of genes regulated by IL-4 in BMDMs. As a result, the promoter region (<1 kb) has more enriched peaks in IL-4-treated BMDMs, suggesting the IL-4 effect most likely takes place in the promoter region (Figure 6A). As expected, M2 signature genes *Arg1*, *Ccl22,* and *Egr2* had more accessible chromatin regions and higher

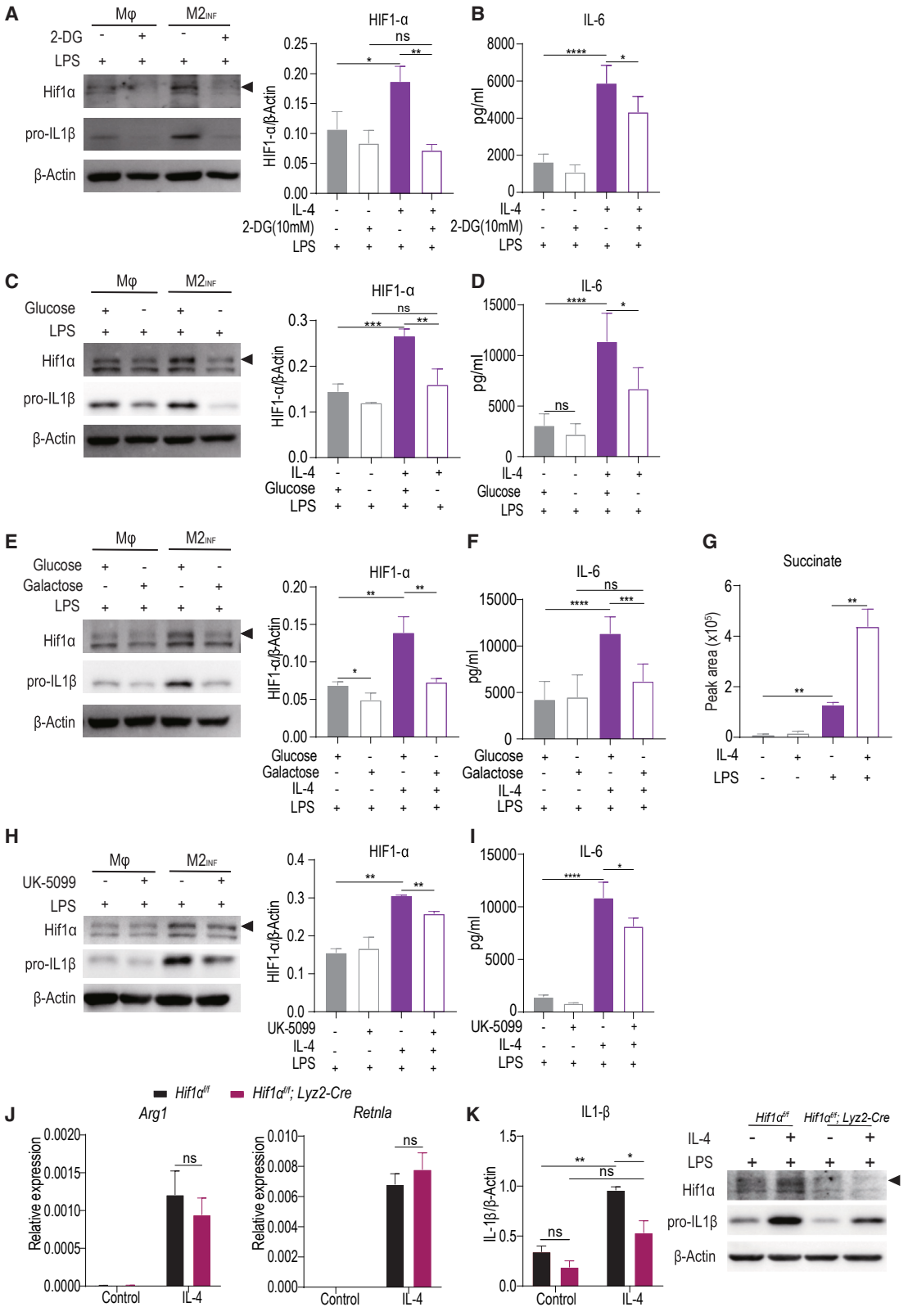

(legend on next page)

gene expression in IL-4-stimulated macrophages (Figure 6B). To gain a global view about the change of the epigenetic landscape, we performed GSEA by concatenating the enriched peaks within 1 Kb of the promoter region. In accordance with RNA-seq results, oxidative phosphorylation, fatty acid oxidation, and retinol metabolism were enriched in IL-4-treated BMDMs (Figures 6C and S6A). Furthermore, both glycolysis and cytokine pathways were enriched in IL-4-treated BMDMs, reinforcing the epigenetic phenotype of $M2_{INF}$ macrophages (Figure 6D). As H3K4me3 is the epigenetic marker enriched at the active promoter region, we further performed an H3K4me3 Cut&Tag to visualize the active promoter. As a result, we found that most glycolysis genes, such as *Hk3, Pfkfb3,* and *Slc1a2 (Glut1)* (Figure 6E), were also enriched with H3K4me3 peaks. Noteworthily, ATAC peaks were also enriched in the promoter region of proinflammatory genes such as *Il6, Il1β,* and *IL12b,* but there was no difference in the H3K4me3 peaks (Figure S6B), suggesting IL-4 treatment opens up the chromatin structure of proinflammatory genes while there is no active transcription activity at basal state. Furthermore, consistent with the essential role of glutamine metabolism in canonical M2 differentiation induced by IL-4, we observed enrichment of H3K4me3 peaks at the promoters of glutamine transporter genes *Slc1a5*, *Slc3a2*, and *Slc7a5*, as well as increased RNA expression levels of *Slc1a5* and *Slc7a5* (Figure S6C).

As H3K4me3 has previously been reported to be the epigenetic landmark of β-glucan-induced trained immunity in macrophages, we further examined whether histone methylation is involved in IL-4-induced non-canonical $M2_{INF}$ macrophages. There was no apparent transcriptional regulation of writers and erasers of H3K4me3 in the IL-4-treated macrophages, as revealed by RNA-seq (Figure S6D). As Wdr5 forms a complex with Mll and Set H3K4 histone methyltransferase family, we knocked down Wdr5 and found that IL-4-induced *Il6* and *Il1β* expression augmentation was partially inhibited (Figures 6F and S6E), suggesting a potential role of H3K4 methylation in $M2_{INF}$ macrophages. Furthermore, inhibition of histone methylation by MTA (pan-methyltransferase inhibitor) impaired IL-4-induced *IL-6* and *IL-1β* gene expression (Figure 6G) and the production of IL-6 and NO (Figure S6F), while MTA did not influence IL-4-induced M2 differentiation (Figure S6G). Putting together the data from the glutamine deficiency experiment, we speculate that IL-4, on the one hand, could induce canonical M2 gene expression via the Gln/α-/Jmjd3 axis.[17,18] On the other hand, IL-4 might induce $M2_{INF}$ macrophages via Wdr5/H3K4me3 axis with persistent epigenetic memory to bolster glycolysis/Hif-1α upon LPS stimulation.

IL-4 induced $M2_{INF}$ macrophages *in vivo*

IL-4c has been reported to induce strong M2 macrophage differentiation *in vivo*.[23] Therefore, to assess whether IL-4c treatment also induces $M2_{INF}$ macrophages *in vivo*, LPS was administered into the peritoneal cavity 1 day after IL-4c injection. The results showed a significant increase in IL-6 and TNF-α levels in both serum (Figure 7A) and peritoneal fluid (Figure S7A) following LPS stimulation. Moreover, IL-4 pretreatment rendered mice more susceptible to LPS-induced sepsis (Figure 7B), presumably due to the heightened cytokine storm induced by IL-4c. Quantitative PCR analysis of purified peritoneal macrophages revealed a significant increase in the basal expression of M2 markers *Arg1* and *Retnla* in IL-4c-pretreated mice (Figure 7C), while these cells still produced higher levels of proinflammatory cytokines upon LPS stimulation (Figure 7D). These results suggest that IL-4 elicits both canonical M2 and non-canonical $M2_{INF}$ macrophages *in vivo*.

Since proinflammatory M1 macrophages have a robust bactericidal capacity, we wondered whether $M2_{INF}$ macrophages also possess enhanced bactericidal ability *in vivo*. We found that IL-4c pretreated mice were more resistant to *Staphylococcus aureus* infection (Figure 7E), suggesting IL-4c pretreatment confers a survival advantage against bactericidal infection. As IL-4 has been reported to modulate myelopoiesis,[24] we further delineated that the IL-4c-induced protection is due to the induction of $M2_{INF}$ macrophages or increase of myelopoiesis. The results showed that short-term IL-4c slightly downregulated the numbers of neutrophils and eosinophils in the peripheral blood (Figure S7B). The drop in neutrophils aligns with the report that IL-4 antagonizes bone marrow egression of neutrophils.[25] Depleting neutrophils with anti-Ly6G antibody in IL-4c-treated mice did not affect IL-4c potentiated survival (Figure S7C), indicating that neutrophils might be dispensable for IL-4c-mediated protection. Adoptive transfer of IL-4-primed $M2_{INF}$ macrophages better protected recipient mice from *S. aureus* infection (Figure 7F), and this protection was abolished in mice receiving IL-4-primed *Hif-1α* MKO BMDMs (Figure 7G). Moreover, $M2_{INF}$ macrophages were also found to have superior phagocytosis and bacterial capacity when incubated with *S. aureus in vitro* (Figure S7D). Taken together, these findings highlight the critical role of the glycolysis/*Hif-1α* axis in enhancing bactericidal capacity in $M2_{INF}$ macrophages *in vivo*.

We further explored the potential role of $M2_{INF}$ macrophages in an OVA-induced allergy model. Compared with control mice, OVA-primed mice were more resistant to *S. aureus* infection (Figure 7H). Furthermore, the bacterial blood colony-forming units (CFUs) are significantly lower in the OVA-primed group, suggesting that acute allergy response induced an enhanced bactericidal effect in mice (Figure S7E). We further confirmed that *Arg1* and *Rentla* were explicitly upregulated in peritoneal macrophages isolated from the OVA-treated group (Figure S7F), confirming the triggering of type 2 response *in vivo*. Moreover, when peritoneal macrophages were stimulated with LPS

Figure 5. Glycolysis/Hif-1α axis is critical for $M2_{INF}$ macrophages

(A–F, H, and I) Control or $M2_{INF}$ macrophages were stimulated with LPS in the presence or absence of (A and B) 2-DG, (C and D) glucose, (E and F) galactose, or (H and I) UK5099. Western blot analysis was performed to determine the levels of Hif-1α and pro-IL-1β, and qPCR was performed to determine *Il6* expression.

(G) The succinate level was determined by LC-MS in control and $M2_{INF}$ macrophages.

(J) Wild-type littermate and Hif-1α MKO BMDMs were treated with IL-4, and qPCR was performed to determine *Arg1* and *Rentla* expression.

(K) Control or $M2_{INF}$ macrophages from wild-type or Hif-1α MKO were stimulated with LPS, and western blot analysis was performed to determine Hif-1α and pro-IL-1β levels. *$p < 0.05$, **$p < 0.01$, ***$p < 0.001$, ****$p < 0.0001$, unpaired, two-tailed Student's t test. Data are representative of two independent experiments with two samples per group (mean ± SD).

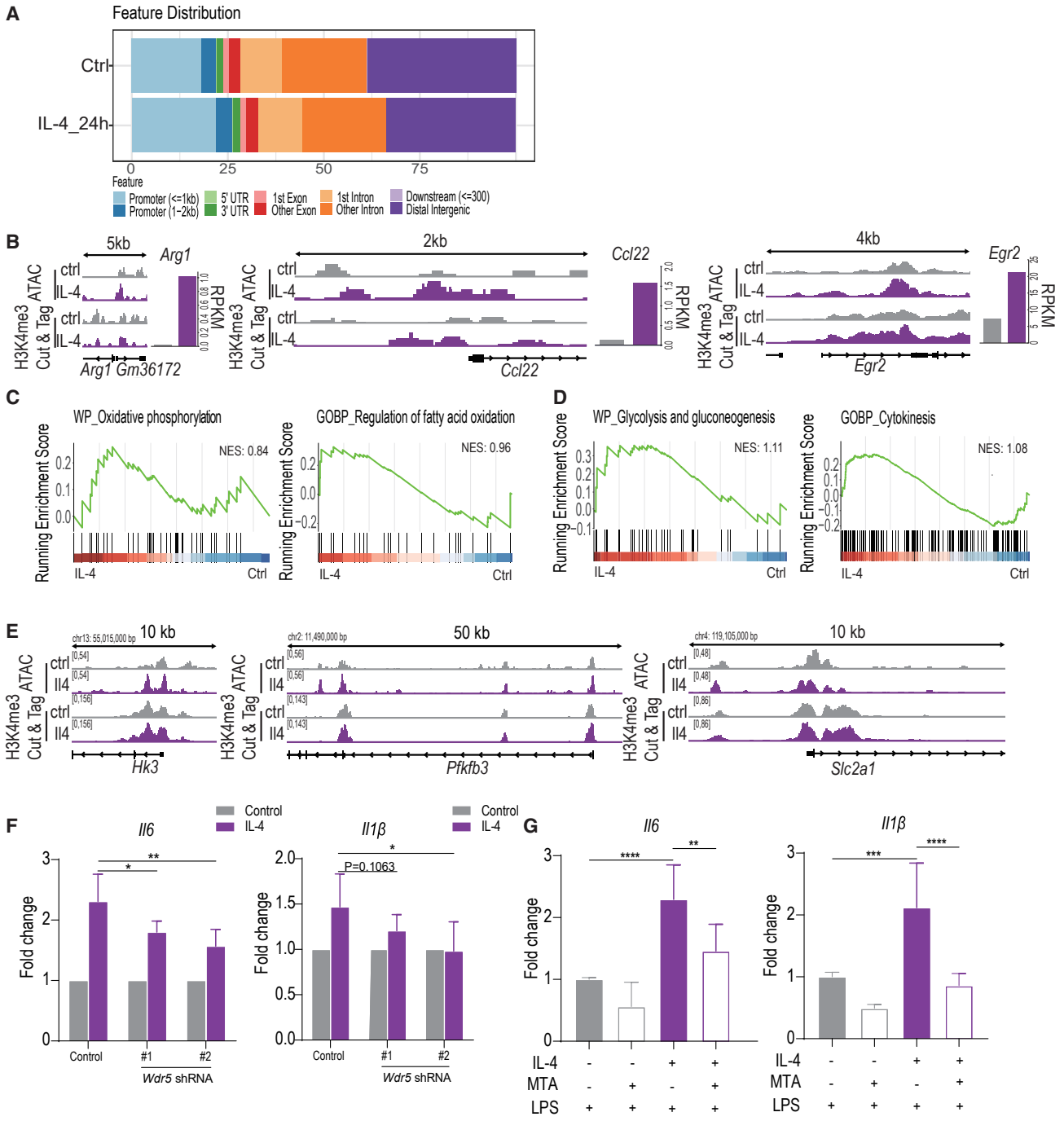

Figure 6. Epigenetic profiles of $M2_{INF}$ macrophages

(A) Distributions of differential ATAC-seq peaks in control and IL-4-treated BMDMs.

(B) Representative ATAC-seq screenshots of M2 marker genes, such as Ccl22, Arg1, and Egr2, in control or IL-4-treated BMDMs. The RPKM of the corresponding gene is depicted in the bar plot.

(C and D) GSEA enrichment of oxidative phosphorylation, fatty acid oxidation (C), and glycolysis and cytokine pathways (D) in IL-4-treated macrophages.

(E) Representative ATAC-seq and H3K4me3 Cut&Tag screenshots of glycolysis genes in control or IL-4-stimulated BMDMs.

(F) Control or *Wdr5* stable knockdown Raw264.7 cells were pretreated with IL-4 for 24 h and stimulated with LPS for 4 h to assess mRNA expression of *Il6* and *Il1β* by qPCR.

(G) qPCR mRNA expression of cytokine genes in BMDMs pretreated with MTA for 30 min followed by 24 h of IL-4 stimulation. The gene expression was determined 4 h post LPS stimulation. *p < 0.05, **p < 0.01, ***p < 0.001, ****p < 0.0001, unpaired, two-tailed Student's t test. Data are representative of three independent experiments with three samples per group (mean ± SD).

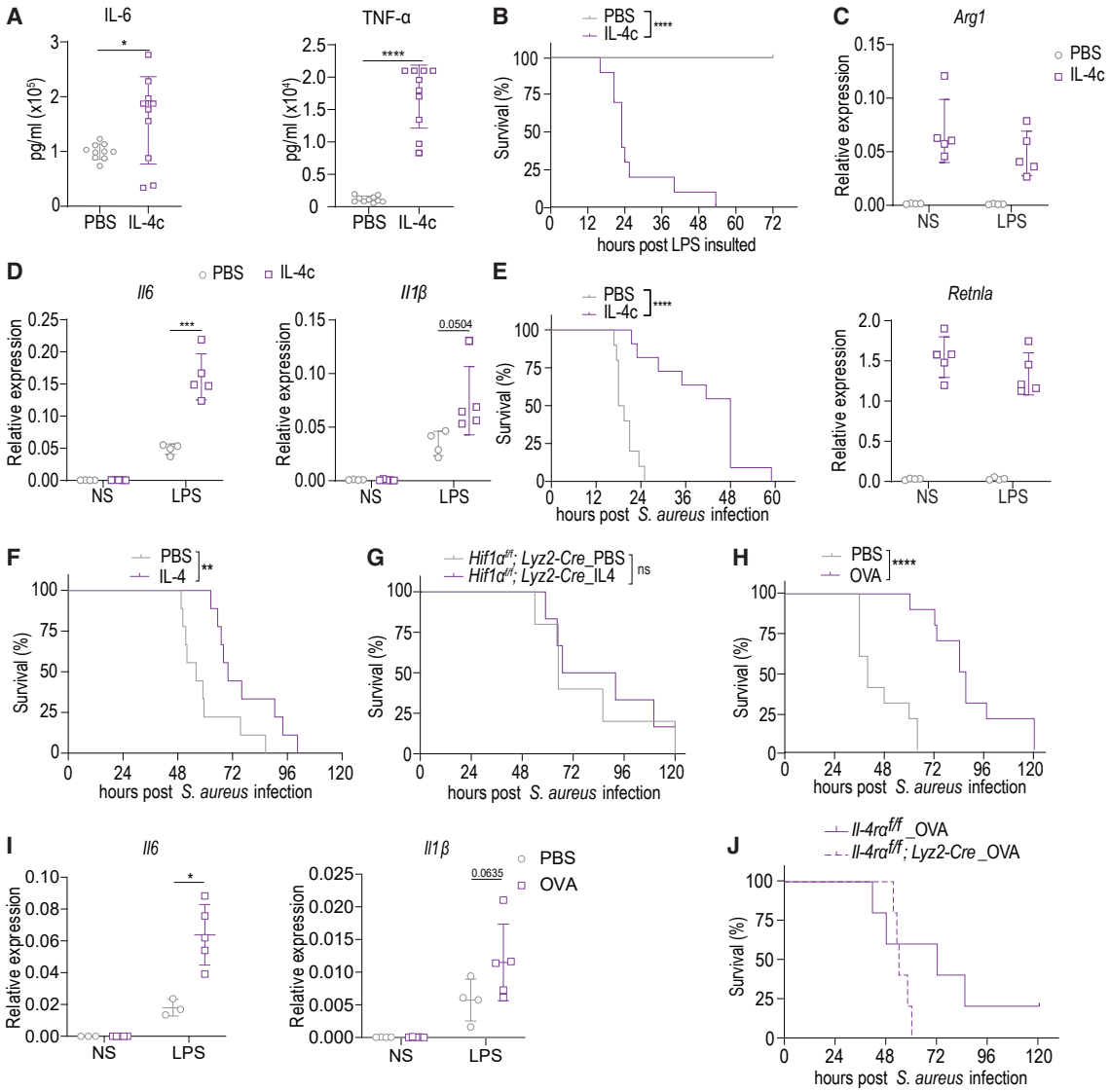

Figure 7. IL-4 induced $M2_{INF}$ macrophages *in vivo*

(A) Serum levels of IL-6 and TNF-α were measured 3 h after LPS injection in mice treated with IL-4c or PBS control.

(B and E) Survival of wild-type mice pretreated with PBS or IL-4c was evaluated after (B) LPS injection or (E) *S. aureus* infection. Results are from two independent experiments with 10 mice per group.

(C) M2 marker gene expression was determined by qPCR in peritoneal macrophages from IL-4c-treated or PBS control mice.

(D) Peritoneal macrophages from IL-4c-treated or PBS control mice were stimulated with LPS *ex vivo* and cytokine gene expression was measured by qPCR.

(F and G) Survival of mice receiving adoptive transfer control or $M2_{INF}$ macrophages from (F) wild-type or (G) *Hif-1*α MKO after *S. aureus* infection.

(H and J) Survival of OVA-Alum primed wild-type mice (H) and IL-4Rα MKO and wild-type littermate mice (J) after *S. aureus* infection. Mice were primed with OVA-Alum twice at day 1 and day 14 and received daily OVA injections from days 21 to 25.

(I) Cytokine gene expression in peritoneal macrophages from OVA-challenged or PBS control mice was measured after LPS stimulation *ex vivo*. *$p < 0.05$, **$p < 0.01$, ***$p < 0.001$, ****$p < 0.0001$, unpaired, two-tailed Student's t test. Data are representative of two independent experiments with eight to 10 mice per group (mean ± SD).

ex vivo, macrophages isolated from the OVA group induced more robust proinflammatory genes (Figure 7I). As type 2 immunity-induced eosinophilia and ILC2 were shown to play roles in protection against bacterial infection,[26] we further examined the role of $M2_{INF}$ macrophages in the OVA-induced allergy model in the *IL-4R*α MKO. Our results demonstrated that *IL-4R*α MKO mice were not protected in the OVA allergy model, highlighting that IL-4Rα is essential in the induction of $M2_{INF}$ macrophages (Figure 7J). Our data suggest that type 2 immune response induces $M2_{INF}$ macrophages, producing more proinflammatory cytokines and more resistance to bacterial infection in animal models.

DISCUSSION

The canonical role of IL-4 in inducing M2 macrophage differentiation and mediating anti-inflammatory responses is well documented. Furthermore, the signaling transduction and pathway involved in IL-4-induced M2 differentiation are well characterized. However, an unrecognized proinflammatory-prone non-canonical feature of IL-4 was left unnoticed. We report that preconditioning with IL-4 induces a non-canonical $M2_{INF}$ macrophage with a robust proinflammatory potential upon microbial stimulation.

Metabolic rewiring and epigenetic control have been reported to play critical roles in canonical M2 macrophage polarization. Jha et al. demonstrated that M2 polarization activates glutamine catabolism and UDP-GlcNAc-associated modules.[27] When macrophages are polarized toward M2 in glutamine-deprived medium or with N-glycosylation inhibitor tunicamycin, M2 polarization and production of Ccl22 are significantly reduced. In addition, Jmjd3, an H3K27me3 demethylase, is upregulated by IL-4 during M2 polarization, and the knockdown of *Jmjd3* also impairs M2 polarization *in vitro*.[28] Furthermore, helminth-induced M2 polarization is significantly reduced in *Jmjd3*$^{-/-}$ mice.[18] α-Ketoglutarate has recently been demonstrated as a central hub bridging glutamine metabolism and Jmjd3-mediated epigenetic programming in M2 macrophages.[17] In addition to glutaminolysis, α-ketoglutarate is also derived as a by-product of the *de novo* serine synthesis pathway via the upregulation of phosphoglycerate dehydrogenase (Phgdh) activity induced by IL-4.[29] Although the Gln/α-KG/Jmjd3 axis has been demonstrated to be crucial for IL-4-mediated M2 differentiation via downregulating H3K27me3, this axis is dispensable for the non-canonical proinflammatory feature induced by IL-4 in macrophages. Our data suggest that IL-4 treatment, on the one hand, induces M2 gene expression via Stat6 and Gln/α-KG/Jmjd3 axes, which opens up the promoter region of M2 signature genes by downregulation of the H3K27me3.[17,18] On the other hand, IL-4 induces $M2_{INF}$ macrophages with a robust proinflammatory feature via recruiting Wdr5 interacting H3K4 methyltransferase, upregulating H3K4me3 around the promoter region of the glycolysis genes, supporting the enhanced glycolysis feature of $M2_{INF}$ macrophages. The H3K4me3 marked promoters serve as epigenetic memory, facilitating a higher transcription activity upon stimulation resulting in a more robust glycolytic switch, Hif-1α stabilization, and subsequent proinflammatory phenotype. Metabolically, IL-4-stimulated macrophages are more energetic with higher basal respiration rate and elevated glycolysis at basal while switching toward robust glycolysis upon stimulation and having higher glycolytic capacity. Inhibition of glycolysis and mitochondrial pyruvate carrier impairs Hif-1α accumulation and subsequent upregulation of proinflammatory cytokine expression. Metabolomics data reveal that IL-4-treated macrophages had elevated one-carbon metabolism, TCA cycle, and glycolysis. The elevated one-carbon metabolism may provide S-adenosyl methionine as a methyl donor for epigenetic modification. Succinate accumulation is involved in Hif-1α stabilization and enhanced IL-1β expression[22] and subsequent H3K4me3 accumulation.[30] Fumarate accumulation is involved in β-glucan-induced H3K4me3 accumulation.[31] Therefore, the elevated intermediate TCA cycle metabolite accumulation in IL-4-stimulated macrophages might impact IL-4-induced $M2_{INF}$ macrophages via epigenetic modification. Moreover, Hif-1α stabilization is indispensable only for the non-canonical arm of IL-4 but does not influence canonical M2 differentiation (Figures 5J and 5K).

It was reported that asthmatic patients had a decreased risk for hospital mortality, septicemia, sepsis, and septic shock across all infections.[12] In a retrospective study, patients who survive *S. aureus* bacteremia have higher numbers of Th2 and fewer Th17 lymphocytes in the blood,[26] suggesting that type 2 immune response might have a beneficial bactericidal effect in humans. In mice, a nematode infection has improved survival from septic bacterial peritonitis.[32] Although the accumulation of mast cells and eosinophils has been suggested to play a role in the bactericidal effect in the acute type 2 immune response, the role of macrophages is mostly unrecognized in this scenario. Acute IL-4c injection has been demonstrated to induce peritoneal macrophage differentiation toward an M2-biased phenotype.[33] However, *ex vivo* stimulation of peritoneal macrophages with IL-4 enhanced IL-6 and TNF-α production upon nematode *Neisseria meningitidis* infection,[34] which is in accordance with the non-canonical $M2_{INF}$ phenotype described here. In addition to IL-4, another type 2 cytokine, IL-13, but not IL-5, could also induce $M2_{INF}$ macrophages *in vitro*.

Moreover, persistent IL-4 stimulation further boosts the proinflammatory response of $M2_{INF}$ macrophages. Therefore, we wonder whether type 2 response could have an acute and chronic effect on macrophages *in vivo*. Mice injected with IL-4c were more susceptible to LPS-induced sepsis and secreted more IL-6 and TNF-α, suggesting acute IL-4 priming could enhance the proinflammatory response *in vivo*. This result is in line with a previous report demonstrating that pretreatment with peritoneal macrophage with IL-4 augments the production of cytokines and chemokines.[35] Moreover, IL-4-pretreatment mice were more resistant to *S. aureus* infection. In addition, the type 2 immune response induced by OVA also renders mice better protection against subsequent bacterial infection (Figure 7H). The peritoneal macrophages from OVA-challenged mice have upregulated IL-6 production compared with control mice (Figure 7I), suggesting that macrophages could acquire a proinflammatory phenotype in the acute type 2 immune response. Therefore, our data suggest that an acute type 2 immune response could induce $M2_{INF}$ macrophages *in vivo*.

In contrast to our finding, Czimmerer et al. reported that IL-4-stimulated macrophages suppressed NLRP3 inflammasome activation and IL-1β secretion upon LPS stimulation in a STAT6-dependent manner.[36] This seemingly contradictory result could be due, at least partly, to the way of BMDM differentiation. Czimmerer et al. used a conditioned medium from L929 cells, while we used recombinant M-CSF for BMDM differentiation. As L929 conditioned medium contains M-CSF and other soluble factors, such as macrophage migration inhibitory factor, osteopontin, Ccl2, and Ccl7, derived from L929, L929 conditioned medium differentiated macrophages were functionally different from recombinant M-CSF-derived macrophages.[37] In addition, they used *Helgmosomoides polygyrus* infection model to induce a type 2 immune response in mice. However, instead of

assessing the role of IL-4 on peritoneal macrophages by bacterial infection, they examined the peritoneal macrophages isolated from *H. polygyrus* infected mice *ex vivo* and showed that peritoneal macrophages from the *H. polygyrus* infected group have lower *Nlrp3* and *Il-1b* expression upon LPS stimulation. In contrast, we adopted a different model to assess whether a prior type 2 response could induce the non-canonical effect of IL-4 *in vivo*, and the collective results point to the same effect that type 2 response causes a more robust proinflammatory response *in vivo* and renders a better protection capacity upon bacterial infection. It is noteworthy that Czimmerer et al. recently reported that IL-4 priming leads to extended synergy upon LPS stimulation through IL-4-induced remodeling, as observed in alveolar macrophages during murine allergic inflammation,[38] which is consistent with the $M2_{INF}$ phenotype. In addition, Lundahl et al. reported that IL-4/IL-13 enhances macrophage OXPHOS activity and induces protective trained immunity against mycobacterial infection.[39] These recent reports and our study demonstrate the biological significance of non-canonical $M2_{INF}$ macrophages and the critical role of IL-4/IL-13-induced protective trained immunity.

Although our current data showcase that Wdr5/H3K4me3-mediated epigenetic modification in the glycolysis genes supports the elevated glycolysis/Hif-1α-axis in $M2_{INF}$ macrophages, there are still questions left to be answered. First, which specific H3K4me3 writer or eraser is directly responsible for the observed H3K4me3 modification? As the known H3K4me3 modifiers did not show significant change at the transcriptional level via RNA-seq analysis, the target H3K4me3 modifier is likely regulated post-translationally via the metabolites change induced by IL-4. Second, which chromatin modifier opens up the promoter region of proinflammatory genes? As these regions are enriched with ATAC peaks but not H3K4me3 peaks, different modifiers seem to be involved in glycolysis and proinflammatory genes. Third, how long is the duration of the phenotype of $M2_{INF}$ macrophages? We have shown that both acute and chronic exposure to IL-4 induced $M2_{INF}$ in macrophages *in vitro*, so it will be therefore essential to assess the duration of the $M2_{INF}$ *in vivo* as the inflammatory-prone consequence might impact the type 2 immune-mediated diseases.

To sum up, we propose that IL-4 induced canonical M2 and non-canonical $M2_{INF}$ macrophages via different epigenetic modifications. The non-canonical trained immunity induced by IL-4 is characterized by Wdr5/H3K4me3 axis, enabling the trained macrophages to be reprogrammed toward elevated glycolysis, leading to Hif-1α stabilization and subsequent more robust proinflammatory phenotype. Due to the association between asthma and acute and chronic inflammatory diseases, we believe a further characterization of IL-4-induced $M2_{INF}$ macrophages will fill the gap between the Th2-biased disease asthma and chronic and acute inflammatory diseases. Thus, our data here provide a fresh vista considering the well-characterized anti-inflammatory cytokine IL-4 and offer an alternative horizon to cope with Th2 disease-associated inflammatory diseases.

Limitations of the study

We demonstrated that the glycolysis/*Hif-1*α-axis is crucial for the induction of non-canonical $M2_{INF}$ macrophages in both *in vitro* and *in vivo* settings. Moreover, we showed that IL-4 stimulation upregulated genes involved in glycolysis at both the transcriptional and epigenetic levels in macrophages. While we revealed that Wdr5-mediated histone methylation is critical for the induction of $M2_{INF}$ macrophages, further investigation is necessary to determine the exact epigenetic modifier responsible. In addition, we investigated the potential role of $M2_{INF}$ macrophages in bolstering enhanced proinflammatory cytokine production and reducing *S. aureus* infection-induced mortality *in vivo*. Although we did not observe alterations in neutrophil counts and found that depleting neutrophils did not impair IL-4c-induced survival enhancement, we cannot exclude the possibility that other cells, such as eosinophils or basophils, might also contribute to the observed enhanced bactericidal effect. IL-4 and other type 2 cytokines may modulate the effect of these granulocytes, thereby enhancing their bactericidal function. Further studies are needed to fully elucidate the role of these cells in the context of $M2_{INF}$-induced enhanced bactericidal capacity.

STAR★METHODS

Detailed methods are provided in the online version of this paper and include the following:

- KEY RESOURCES TABLE
- RESOURCE AVAILABILITY
  - Lead contact
  - Materials availability
  - Data and code availability
- EXPERIMENTAL MODEL AND SUBJECT DETAILS
  - Animals
  - IL4c administration and LPS induced sepsis
  - OVA-induced allergy model
- METHOD DETAILS
  - BMDM adoptive transfer model
  - Bone-marrow-derived macrophage (BMDM) culture and differentiation
  - Quantitative real-time PCR
  - ELISA and lactate measurement
  - NO measurement
  - *In vitro* phagocytosis and killing assay
  - Assay for transposase-accessible chromatin with high-throughput sequencing (ATAC-seq)
  - CUT&Tag library preparation
  - RNA isolation and sequence
  - Metabolomics
  - Ly6G depletion assay
  - Western blot
  - RNA-seq data analysis
  - CUT&Tag-seq and ATAC-seq data analysis
- QUANTIFICATION AND STATISTICAL ANALYSIS

SUPPLEMENTAL INFORMATION

Supplemental information can be found online at https://doi.org/10.1016/j.celrep.2023.112471.

ACKNOWLEDGMENTS

Funding was received from the following sources: National Natural Science Foundation of China grants 32161133020 and 32070904 (S.-C.C.), Fundamental Research Funds for the Central Universities 20720220003 (S.-C.C.), start-up fund of Xiamen University (S.-C.C.), European Research Council Starting Grant 802773-MitoGuide (P.-C.H.), SNSF project grant 31003A_182470 (P.-C.H.), Cancer Research Institute (P.-C.H.), American Cancer Society RSG-22-135-01-IBCD (S.C.-C.H.), Melanoma Research Foundation Career Development Award (S.C.-C.H.), Andrew McDonough B+ Foundation Grant Award (S.C.-C.H.), Case GI SPORE DRP grant 5P50CA150964-08 (S.C.-C.H.), Cancer Research Institute CLIP Investigator Award (S.C.-C.H.), and Comprehensive Cancer Center American Cancer SocietyPilot Grants IRG-91-022-19 and IRG-16-186-21(S.C.-C.H.).

AUTHOR CONTRIBUTIONS

Conceptualization, S.-C.C.; methodology, B.D., Q.G., L.Z., J.Z., Q.Z., Y.H., J.L., and S.-C.C.; formal analysis, B.D., Q.G., L.Z., J.Z., and S.-C.C.; investigation, B.D., Q.G., L.Z., S.L., J.Z., Y.H., S.C.-C.H., P.-C.H., and S.-C.C.; funding acquisition, S.-C.C.; supervision, S.-C.C.; writing – original draft, D.B., J.Z., and S.-C.C.; writing – review & editing, D.B., Q.G., S.L., J.Z., N.X., W.-H.L., K.M., S.L., J.H., S.C.-C.H., P.-C.H., and S.-C.C.

DECLARATION OF INTERESTS

The authors declare no competing interests.

Received: November 2, 2022
Revised: March 8, 2023
Accepted: April 19, 2023
Published: May 6, 2023

REFERENCES

1. Fujieda, S., Zhang, K., and Saxon, A. (1995). IL-4 plus CD40 monoclonal antibody induces human B cells gamma subclass-specific isotype switch: switching to gamma 1, gamma 3, and gamma 4, but not gamma 2. J. Immunol. *155*, 2318–2328.
2. Lebman, D.A., and Coffman, R.L. (1988). Interleukin 4 causes isotype switching to IgE in T cell-stimulated clonal B cell cultures. J. Exp. Med. *168*, 853–862. https://doi.org/10.1084/jem.168.3.853.
3. Stuart, P.M., Zlotnik, A., and Woodward, J.G. (1988). Induction of class I and class II MHC antigen expression on murine bone marrow-derived macrophages by IL-4 (B cell stimulatory factor 1). J. Immunol. *140*, 1542–1547.
4. Sarfati, M., Fournier, S., Christoffersen, M., and Biron, G. (1990). Expression of CD23 antigen and its regulation by IL-4 in chronic lymphocytic leukemia. Leuk. Res. *14*, 47–55. https://doi.org/10.1016/0145-2126(90)90145-Y.
5. Sonoda, Y. (1994). Interleukin-4–a dual regulatory factor in hematopoiesis. Leuk. Lymphoma *14*, 231–240. https://doi.org/10.3109/10428199409049673.
6. Locati, M., Curtale, G., and Mantovani, A. (2020). Diversity, mechanisms, and significance of macrophage plasticity. Annu. Rev. Pathol. *15*, 123–147. https://doi.org/10.1146/annurev-pathmechdis-012418-012718.
7. Orecchioni, M., Ghosheh, Y., Pramod, A.B., and Ley, K. (2019). Macrophage polarization: different gene signatures in M1(LPS+) vs. Classically and M2(LPS-) vs. Alternatively activated macrophages. Front. Immunol. *10*, 1084. https://doi.org/10.3389/fimmu.2019.01084.
8. Sica, A., and Mantovani, A. (2012). Macrophage plasticity and polarization: in vivo veritas. J. Clin. Invest. *122*, 787–795. https://doi.org/10.1172/jci59643.
9. Genard, G., Lucas, S., and Michiels, C. (2017). Reprogramming of tumor-associated macrophages with anticancer therapies: radiotherapy versus chemo- and immunotherapies. Front. Immunol. *8*, 828. https://doi.org/10.3389/fimmu.2017.00828.
10. Kammoun, H.L., and Febbraio, M.A. (2014). Macrophage polarization in obesity and type 2 diabetes: weighing down our understanding of macrophage function? Cell Metab. *19*, 1–2. https://doi.org/10.3389/fimmu.2014.00470.
11. Bäck, M., Yurdagul, A., Jr., Tabas, I., Öörni, K., and Kovanen, P.T. (2019). Inflammation and its resolution in atherosclerosis: mediators and therapeutic opportunities. Nat. Rev. Cardiol. *16*, 389–406.
12. Zein, J.G., Love, T.E., and Erzurum, S.C. (2017). Asthma is associated with a lower risk of sepsis and sepsis-related mortality. Am. J. Respir. Crit. Care Med. *196*, 787–790. https://doi.org/10.1164/rccm.201608-1583le.
13. Bantulà, M., Roca-Ferrer, J., Arismendi, E., and Picado, C. (2021). Asthma and obesity: two diseases on the rise and bridged by inflammation. J. Clin. Med. *10*, 169.
14. Peters, U., Dixon, A.E., and Forno, E. (2018). Obesity and asthma. J. Allergy Clin. Immunol. *141*, 1169–1179.
15. Bailey, J.D., Diotallevi, M., Nicol, T., McNeill, E., Shaw, A., Chuaiphichai, S., Hale, A., Starr, A., Nandi, M., Stylianou, E., et al. (2019). Nitric oxide modulates metabolic remodeling in inflammatory macrophages through TCA cycle regulation and itaconate accumulation. Cell Rep. *28*, 218–230.e7. https://doi.org/10.1016/j.celrep.2019.06.018.
16. Van den Bossche, J., Baardman, J., Otto, N.A., van der Velden, S., Neele, A.E., van den Berg, S.M., Luque-Martin, R., Chen, H.-J., Boshuizen, M.C.S., Ahmed, M., et al. (2016). Mitochondrial dysfunction prevents repolarization of inflammatory macrophages. Cell Rep. *17*, 684–696. https://doi.org/10.1016/j.celrep.2016.09.008.
17. Liu, P.-S., Wang, H., Li, X., Chao, T., Teav, T., Christen, S., Di Conza, G., Cheng, W.-C., Chou, C.-H., Vavakova, M., et al. (2017). α-ketoglutarate orchestrates macrophage activation through metabolic and epigenetic reprogramming. Nat. Immunol. *18*, 985–994. https://doi.org/10.1038/ni.3796.
18. Satoh, T., Takeuchi, O., Vandenbon, A., Yasuda, K., Tanaka, Y., Kumagai, Y., Miyake, T., Matsushita, K., Okazaki, T., Saitoh, T., et al. (2010). The Jmjd3-Irf4 axis regulates M2 macrophage polarization and host responses against helminth infection. Nat. Immunol. *11*, 936–944. https://doi.org/10.1038/ni.1920.
19. He, L., Jhong, J.-H., Chen, Q., Huang, K.-Y., Strittmatter, K., Kreuzer, J., DeRan, M., Wu, X., Lee, T.-Y., Slavov, N., et al. (2021). Global characterization of macrophage polarization mechanisms and identification of M2-type polarization inhibitors. Cell Rep. *37*, 109955. https://doi.org/10.1016/j.celrep.2021.109955.
20. Viola, A., Munari, F., Sánchez-Rodríguez, R., Scolaro, T., and Castegna, A. (2019). The metabolic signature of macrophage responses. Front. Immunol. *10*, 1462. https://doi.org/10.3389/fimmu.2019.01462.
21. Cheng, S.-C., Quintin, J., Cramer, R.A., Shepardson, K.M., Saeed, S., Kumar, V., Giamarellos-Bourboulis, E.J., Martens, J.H.A., Rao, N.A., Aghajanirefah, A., et al. (2014). mTOR- and HIF-1α-mediated aerobic glycolysis as metabolic basis for trained immunity. Science *345*, 1250684. https://doi.org/10.1126/science.1250684.
22. Tannahill, G.M., Curtis, A.M., Adamik, J., Palsson-McDermott, E.M., McGettrick, A.F., Goel, G., Frezza, C., Bernard, N.J., Kelly, B., Foley, N.H., et al. (2013). Succinate is an inflammatory signal that induces IL-1β through HIF-1α. Nature *496*, 238–242. https://doi.org/10.1038/nature11986.
23. Huang, S.C.-C., Smith, A.M., Everts, B., Colonna, M., Pearce, E.L., Schilling, J.D., and Pearce, E.J. (2016). Metabolic reprogramming mediated by the mTORC2-IRF4 signaling Axis is essential for macrophage alternative activation. Immunity *45*, 817–830. https://doi.org/10.1016/j.immuni.2016.09.016.
24. Snoeck, H.W., Lardon, F., van Bockstaele, D.R., and Peetermans, M.E. (1993). Effects of interleukin-4 (IL4) on myelopoiesis: studies on highly purified CD34+ hematopoietic progenitor cells. Leukemia *7*, 625–629. https://doi.org/10.1007/bf01700376.

25. Woytschak, J., Keller, N., Krieg, C., Impellizzieri, D., Thompson, R.W., Wynn, T.A., Zinkernagel, A.S., and Boyman, O. (2016). Type 2 interleukin-4 receptor signaling in neutrophils antagonizes their expansion and migration during infection and inflammation. Immunity *45*, 172–184. https://doi.org/10.1016/j.immuni.2016.06.025.

26. Krishack, P.A., Louviere, T.J., Decker, T.S., Kuzel, T.G., Greenberg, J.A., Camacho, D.F., Hrusch, C.L., Sperling, A.I., and Verhoef, P.A. (2019). Protection against Staphylococcus aureus bacteremia-induced mortality depends on ILC2s and eosinophils. JCI Insight *4*, e124168. https://doi.org/10.1172/jci.insight.124168.

27. Jha, A.K., Huang, S.C.-C., Sergushichev, A., Lampropoulou, V., Ivanova, Y., Loginicheva, E., Chmielewski, K., Stewart, K.M., Ashall, J., Everts, B., et al. (2015). Network integration of parallel metabolic and transcriptional data reveals metabolic modules that regulate macrophage polarization. Immunity *42*, 419–430. https://doi.org/10.1016/j.immuni.2015.02.005.

28. Ishii, M., Wen, H., Corsa, C.A.S., Liu, T., Coelho, A.L., Allen, R.M., Carson, W.F., Cavassani, K.A., Li, X., Lukacs, N.W., et al. (2009). Epigenetic regulation of the alternatively activated macrophage phenotype. Blood *114*, 3244–3254. https://doi.org/10.1182/blood-2009-04-217620.

29. Wilson, J.L., Nägele, T., Linke, M., Demel, F., Fritsch, S.D., Mayr, H.K., Cai, Z., Katholnig, K., Sun, X., Fragner, L., et al. (2020). Inverse data-driven modeling and multiomics analysis reveals Phgdh as a metabolic checkpoint of macrophage polarization and proliferation. Cell Rep. *30*, 1542–1552.e7. https://doi.org/10.1016/j.celrep.2020.01.011.

30. Keating, S.T., Groh, L., van der Heijden, C.D.C.C., Rodriguez, H., Dos Santos, J.C., Fanucchi, S., Okabe, J., Kaipananickal, H., van Puffelen, J.H., Helder, L., et al. (2020). The Set7 lysine methyltransferase regulates plasticity in oxidative phosphorylation necessary for trained immunity induced by β-glucan. Cell Rep. *31*, 107548. https://doi.org/10.1016/j.celrep.2020.107548.

31. Arts, R.J.W., Novakovic, B., Ter Horst, R., Carvalho, A., Bekkering, S., Lachmandas, E., Rodrigues, F., Silvestre, R., Cheng, S.-C., Wang, S.-Y., et al. (2016). Glutaminolysis and fumarate accumulation integrate immunometabolic and epigenetic programs in trained immunity. Cell Metab. *24*, 807–819. https://doi.org/10.1016/j.cmet.2016.10.008.

32. Sutherland, R.E., Xu, X., Kim, S.S., Seeley, E.J., Caughey, G.H., and Wolters, P.J. (2011). Parasitic infection improves survival from septic peritonitis by enhancing mast cell responses to bacteria in mice. PLoS One *6*, e27564. https://doi.org/10.1371/journal.pone.0027564.

33. Jenkins, S.J., Ruckerl, D., Thomas, G.D., Hewitson, J.P., Duncan, S., Brombacher, F., Maizels, R.M., Hume, D.A., and Allen, J.E. (2013). IL-4 directly signals tissue-resident macrophages to proliferate beyond homeostatic levels controlled by CSF-1. J. Exp. Med. *210*, 2477–2491. https://doi.org/10.1084/jem.20121999.

34. Varin, A., Mukhopadhyay, S., Herbein, G., and Gordon, S. (2010). Alternative activation of macrophages by IL-4 impairs phagocytosis of pathogens but potentiates microbial-induced signalling and cytokine secretion. Blood *115*, 353–362. https://doi.org/10.1182/blood-2009-08-236711.

35. Major, J., Fletcher, J.E., and Hamilton, T.A. (2002). IL-4 pretreatment selectively enhances cytokine and chemokine production in lipopolysaccharide-stimulated mouse peritoneal macrophages. J. Immunol. *168*, 2456–2463. https://doi.org/10.4049/jimmunol.168.5.2456.

36. Czimmerer, Z., Daniel, B., Horvath, A., Rückerl, D., Nagy, G., Kiss, M., Peloquin, M., Budai, M.M., Cuaranta-Monroy, I., Simandi, Z., et al. (2018). The transcription factor STAT6 mediates direct repression of inflammatory enhancers and limits activation of alternatively polarized macrophages. Immunity *48*, 75–90.e6. https://doi.org/10.1016/j.immuni.2017.12.010.

37. Heap, R.E., Marín-Rubio, J.L., Peltier, J., Heunis, T., Dannoura, A., Moore, A., and Trost, M. (2021). Proteomics characterisation of the L929 cell supernatant and its role in BMDM differentiation. Life Sci. Alliance *4*, e202000957. https://doi.org/10.26508/lsa.202000957.

38. Czimmerer, Z., Halasz, L., Daniel, B., Varga, Z., Bene, K., Domokos, A., Hoeksema, M., Shen, Z., Berger, W.K., Cseh, T., et al. (2022). The epigenetic state of IL-4-polarized macrophages enables inflammatory cistromic expansion and extended synergistic response to TLR ligands. Immunity *55*, 2006–2026.e6. https://doi.org/10.1016/j.immuni.2022.10.004.

39. Lundahl, M.L.E., Mitermite, M., Ryan, D.G., Case, S., Williams, N.C., Yang, M., Lynch, R.I., Lagan, E., Lebre, F.M., Gorman, A.L., et al. (2022). Macrophage innate training induced by IL-4 and IL-13 activation enhances OXPHOS driven anti-mycobacterial responses. Elife *11*, e74690. https://doi.org/10.7554/elife.74690.

STAR★METHODS

KEY RESOURCES TABLE

REAGENT or RESOURCE	SOURCE	IDENTIFIER
Antibodies		
β-Actin	Abcam	Cat# ab8226, RRID: AB_306371
Pfkfb3	Signalway Antibody	Cat# 49656, RRID: AB_2936227
Hexokinase1	Abclonal	Cat# A10886, RRID: AB_2758295
Hexokinase3	Abclonal	Cat# A8428, RRID: AB_2769796
Glut1	Abclonal	Cat# A11727, RRID: AB_2861637
Histone H3	Abclonal	Cat# A2348, RRID: AB_2631273
Hif1α	Abclonal	Cat# A11945, RRID: AB_2758885
Aldolase A	CST	Cat# 8060, RRID: AB_2797635
Enolase-1	CST	Cat# 3810, RRID: AB_2246524
Stat6	CST	Cat# 5397; RRID: AB_11220421
Histone H3K4me$_3$	CST	Cat# 9751, RRID: AB_2616028
Wdr5	Abclonal	Cat# A2023, RRID: AB_2764047
IL-1 beta	Abcam	Cat# ab234437, RRID: AB_2936228
Goat Anti-Rabbit IgG	Signalway Antibody	Cat# L3012, RRID: AB_895483
Cd86	BioLegend	Cat# 105007, RRID: AB_313150
Mhc class II	Thermo Fisher Scientific	Cat# 15-5321-82, RRID: AB_468800
anti-mouse IL-4 antibody	Bio X Cell	Cat# BE0045, RRID: AB_1107707
anti-mouse Ly6G antibod	Bio X Cell	Cat# BE0075-1, RRID: AB_1107721
Rat IgG2b isotype control	Bio X Cell	Cat# BE0090, RRID: AB_1107780
Bacterial and virus strains		
Staphylococcus aureus	ATCC	ATCC 29213
Chemicals, peptides, and recombinant proteins		
Alum	Sigma-Aldrich	# A6435
OVA	Sigma-Aldrich	# A5253
Galactose	Sigma-Aldrich	#G0750
DMSO	Sigma-Aldrich	#V900090
Dihydrochloride Sulfanilamide	Sigma-Aldrich	#S9251
N-(1-Naphthyl) ethylenediamine	Sigma-Aldrich	#N9125

(*Continued on next page*)

Continued

REAGENT or RESOURCE	SOURCE	IDENTIFIER
Glucose	Sigma-Aldrich	#G7021
2-deoxy glucose	Sigma-Aldrich	#D8375
Mouse M-CSF	Novoprotein	# CD34
Mouse IL-4 (C-6His)	Novoprotein	# CK74
Mouse IL-13 (C-6His)	Novoprotein	# CX57
Mouse IFN gamma (C-6His)	Novoprotein	# CM41
Lipopolysaccharides (LPS) from E. coli	Invivogen	# tlrl-pb5lps
Mouse Tnf alpha ELISA RSG 20 X 96 TE	Invitrogen	# 88-7324-88
Mouse IL-6 ELISA RSG 20 X 96 TE	Invitrogen	# 88-7064-88
SYBR	Accurate biology	# AG11701
Evo M-MLV reverse transcriptase	Accurate biology	# AG11605
recombinant RNase inhibitor	Accurate biology	# AG11608
Amplex Red	Alfachem	# 119171-73-2
Penicillin-Streptomycin	Gibco	# 15140-122
GlutaMAX™ - I (100X)	Gibco	# 2085268
Opti-MEM	Gibco	# 31985070
PBS	Hyclone	# SH30256.01
DMEM	Hyclone	# SH30243.01
Sodium dodecyl sulfate	Sangon Biotech	# A100227
Glycine	Sangon Biotech	# A110167
Tris	Sangon Biotech	# 77-86-1
Bovine serum albumin	Sangon Biotech	# A600332
Protease and phosphatase inhibitor	Bestbio	# BB-3374
5′-Methylthioadenosine	MedChemExpress	# HY-16938
UK-5099	MedChemExpress	# HY-15475
GSK-J4	MedChemExpress	# HY-15648B
BPTES	MedChemExpress	# HY-12683
dNTP	Beyotime	#D7366
Critical commercial assays		
CUT&Tag 3.0 kit	Novoprotein	#N259-YH01-01A
Agencourt AMPure XP kit	Beckman Coulter	#A63880
TruePrep DNA Library Prep Kit V2	Vazyme	#TD501
Deposited data		
RNA-seq	This paper	GSE184811
ATAC-seq	This paper	GSE196099
CUT & Tag-seq	This paper	GSE196099
Experimental models: Organisms/strains		
Mouse: C57BL/6J	The Jackson Laboratory	JAX: 000664
Mouse: IL4Ra-flox	Gempharmatech	Strain NO. T005747
Mouse: Hif1a-flox	Gempharmatech	Strain NO. T007239
Oligonucleotides		
Primers for real-time PCR	This paper	N/A
ShRNA sequences	This paper	N/A
Software and algorithms		
GraphPad Prism v.8	Graphpad	https://www.graphpad.com/
FlowJo v.10	Flow Jo	https://www.flowjo.com/
ImageJ	NIH	https://imagej.nih.gov/ij/

RESOURCE AVAILABILITY

Lead contact

Further information and requests for reagents may be directed to and will be fulfilled by the lead contact, Shih-Chin Cheng (jamescheng@xmu.edu.cn).

Materials availability

This study did not generate new unique reagents.

Data and code availability

RNA-seq, ATAC-seq, and Cut &Tag-seq data in this study have been deposited at GEO and are publicly available. The accession number is listed in the key resources table.

This paper does not report original code.

Any additional information required to reanalyze the data reported in this paper is available from the lead contact upon request.

EXPERIMENTAL MODEL AND SUBJECT DETAILS

Animals

Wild-type C57BL/6 mice (Xiamen University Laboratory Animal Center), *Hif-1α*$^{f/f}$ (Kind gift from Dr. Wen-Hsien Liu, Xiamen University), IL-4Rαf/f (GermPharmatech), and *Lyz2-cre* mice (GermPharmatech) were housed in specific pathogen-free conditions at the Xiamen University Laboratory Animal Center. Institutional Animal Care and Use Committee approved all mouse experiments in accordance with good animal practice defined by the Xiamen University Laboratory Animal Center.

IL4c administration and LPS induced sepsis

To administer IL-4 complex (IL-4c), 5 μg of recombinant mouse IL-4 was complexed to 25 μg of anti-mouse IL-4 antibody (BioXCell,11B11) and diluted in 200 μl of PBS before being given intraperitoneally. Twenty-four hours after IL-4c administration, mice were injected with 20 mg/kg LPS to induce sepsis. Serum was harvested from the caudal tail 2 hours post-LPS injection, and ELISA was used to determine IL-6 and TNF-α levels in the serum according to the manufacturer's instructions. Mice survival after LPS injection was monitored for 6 days.

OVA-induced allergy model

C57BL/6 mice were used to induce the OVA-induced allergy model. The mice were intraperitoneally injected with a solution containing 100 μg of OVA (catalog number Sigma, A5253) absorbed to 10 % Alum (catalog number Sigma, A6435) at a final volume ratio of OVA to Alum of 1:1 on days 0 and 14. From days 21 to 25, the mice were intraperitoneally injected with 0.1 mg of OVA in 200 μl of PBS. On day 27, the mice were intraperitoneally injected with Staphylococcus aureus at a dose of 5×10^3 CFU in 200 μL PBS per mouse, and whole blood was collected from the caudal tail on day 26 for calculating the CFU.

METHOD DETAILS

BMDM adoptive transfer model

BMDMs were treated with 20 ng/ml of IL-4 for 24 hours. Next, 7.5×10^5 IL-4-primed or control BMDM cells were adoptively transferred to mice via intravenous injection. The mice were then infected with 6×10^6 CFU of Staphylococcus aureus via intranasal injection and monitored for survival.

Bone-marrow-derived macrophage (BMDM) culture and differentiation

Bone marrow-derived macrophages (BMDMs) were obtained by harvesting bone marrow cells from the femurs and tibia of 6–8-week-old C56BL6/J mice. The cells were then differentiated in DMEM supplemented with 10% FBS and 40 ng/ml of recombinant mouse M-CSF. On day 3, a fresh medium containing half the original volume of 40 ng/ml of recombinant M-CSF was added to the cell culture. At day 6, the differentiated BMDMs were detached, counted, and reseeded to the cell culture plate for subsequent experiments.

To conduct polarization experiments with BMDMs, 20 ng/ml LPS and 100 ng/ml IFNγ were added to induce M1 macrophage polarization, while 20 ng/ml IL-4 was used to induce M2 polarization. For short-term assessment of type 2 cytokine effects, BMDMs were cultured with 20 ng/ml of IL-4, IL-5, or IL-13 for 24 hours, then washed with PBS and stimulated with 100 ng/ml LPS to assess cytokine production capacity. For long-term assessment, BMDMs were first cultured with 20 ng/ml IL-4 for 24 hours, washed with PBS, and refreshed with 10 ng/ml M-CSF containing DMEM for an additional 5 days before being harvested for subsequent functional assessment.

To assess the signaling pathways involved in IL-4-induced canonical and non-canonical effects, BMDMs were pre-incubated with various inhibitors for 30 minutes prior to IL-4 stimulation. BMDMs were washed with PBS 24 hours after IL-4 stimulation and harvested for subsequent functional assessment.

Quantitative real-time PCR

For quantitative RT-PCR, total mRNA was extracted with oligo-dT magnetic beads. In short, RNA was extracted by magnetic beads conjugated with Oligo-dT18. Isolated RNA was reverse transcribed into cDNA using dNTP (Beyotime, D7366)/oligodT mix, RNA transcriptase (Accurate Biology, AG11605), and RNase inhibitor (Accurate Biology, AG11608). qPCR was performed using the SYBR Green method (Accurate Biology, AG11701). Relative expression levels were calculated using the ΔCT method and normalized to the expression of the β2M housekeeping gene. The primer sequences used are listed in Table S1.

ELISA and lactate measurement

Cytokine levels in culture supernatant or mice serum were determined by TNF-α (Invitrogen; 88-7324-88) and IL-6 (Invitrogen; 88-7064-88) ELISA kits following the instructions of the manufacturer. Lactate measurements were performed by diluting the cellular supernatant with PBS, then mixing the diluent with the mixture containing Amplex Red, HRP, and lactate oxidase for 10 min. Fluorescence was detected at excitation wavelength at 528 nm and emission wavelength at 590 nm by a fluorescence plate reader.

NO measurement

The culture supernatant was mixed with a 1:1 ratio of ethylenediamine dihydrochloride solution and sulfanilamide solution, and absorbance was measured at 540 nm to determine the NO concentration.

In vitro phagocytosis and killing assay

BMDMs were seeded into each well of a 24-well plate (5×10^5 cells/well). BMDMs were then incubated with live S. aureus at a ratio of one macrophage to two bacteria for 3 hours. After incubation, non-phagocytosed bacteria were removed by washing the cells three times with PBS. BMDMs were then treated with gentamicin-containing medium (400 ng/ml) for 30 minutes to eliminate any remaining extracellular and cell surface-attached bacteria.

For the phagocytosis assay, macrophages were lysed using 100 μl of 0.1% Triton-X100 in PBS. The resulting cell lysates were serially diluted in PBS, and aliquots were aseptically plated and cultured on LB agar plates at 37°C. After 14-18 hours of incubation, bacterial colonies were counted, and the results were expressed as colony-forming units (CFUs) per 5×10^5 BMDMs.

For the killing assay, macrophages were cultured for an additional 2.5 hours before determining the CFU count. Killing efficiency was calculated using the following equation: (CFU at 3h - CFU at 6h)/(CFU at 3 h) × 100 %.

Assay for transposase-accessible chromatin with high-throughput sequencing (ATAC-seq)

ATAC-seq was carried out using the TruePrep DNA Library Prep Kit V2 for Illumina (Vazyme, TD501) with minor modifications. Briefly, 30,000 cells were spun at 500 g for 5 min and then lysed for 10 min at 4°C with pre-cold lysis buffer (10 mM Tris-HCl, pH 7.4, 10 mM NaCl, 3 mM MgCl2, and 0.1% IGEPAL CA-630). Nuclei were harvested for transposition reaction. After tagmentation, DNA was purified using the Agencourt AMPure XP kit (Beckman Coulter, A63880). To reduce GC and size bias, we determined the final PCR cycles using qPCR to allow library amplification to be stopped before saturation. We performed initial amplifications for five cycles, after which we took an aliquot of the PCR reaction and added 10 μL of the PCR cocktail with SYBR Green at a final concentration of 0.3×. We ran this reaction for 25 cycles to calculate the additional cycles required for the remaining 45 μL reaction. We amplified library fragments for 12-13 cycles, and the libraries underwent double size selection for 300-500 bp DNA fragments. Fragment distribution of libraries was assessed with Agilent 4200. The library preparations were sequenced on an Illumina Hiseq platform, and 150 bp paired-end reads were generated.

CUT&Tag library preparation

CUT&Tag libraries were prepared using the NovoNGS® CUT&Tag 3.0 kit (N259-YH01-01A, Novoprotein). Briefly, 100,000 sorted cells were captured by Con A beads. Cells-beads complexes were incubated with primary H3K4me3 antibody (Cell Signal Technology CST 9751) and secondary rabbit IgG antibody (Abcam ab171870) at room temperature. The unbound antibodies and cells-beads complexes were washed with antibody buffer, and Tn5-pA/G was added to the cell-beads complex for transposition reaction at 37°C. The DNA fragments were extracted and purified using extraction beads.

RNA isolation and sequence

RNA from cells was isolated using the RNAprep Pure Cell/Bacteria Kit (TIANGEN) following the manufacturer's instructions. RNA samples were quantified using Qubit and an Agilent Bioanalyzer for RNA integrity assessment. All samples had an RNA integrity number (RIN) of approximately 10. Following the manufacturer's recommendations, sequencing libraries were generated using the NEBNext® UltraTM RNA Library Prep Kit for Illumina® (NEB, USA), and index codes were added to attribute sequences to each sample. The clustering of the index-coded samples was performed on a cBot Cluster Generation System using the TruSeq PE Cluster Kit v3-cBot-HS (Illumina) according to the manufacturer's instructions. After cluster generation, the library was sequenced on an Illumina Novaseq platform, and 150 bp paired-end reads were generated.

Metabolomics

To conduct metabolite tracing experiments, 2×10^6 bone marrow-derived macrophages were seeded in a 6-well plate and treated as described above. For the metabolite tracing experiment, the DMEM was replaced with glucose-free medium supplemented with

12.5 mM U-[^{13}C]-glucose (Cambridge Isotope Laboratories) with or without 4 mM glutamine (Gibco). For metabolite extraction, cells were washed three times with pre-cold PBS, and then the plates were put on ice. 1 ml of extraction buffer (volume ratio 4:1 methanol/water) was added to the cells, which were then scraped on ice. The lysate was transferred to a 2 ml tube and vortexed for 30 seconds, followed by additional 10 minutes sonication in the ice bath. The mixture was immediately frozen in a liquid nitrogen tank and then centrifuged at 13,000 rpm for 15 min at 4°C. Finally, supernatants were transferred to a new tube and lyophilized.

For metabolite analysis, liquid chromatography with SCIEX Exion LC AD was prepared, and all chromatographic separations were performed with a Millipore ZIC-pHILIC column (5 μm, 2.1× 100 mm internal dimensions, PN: 1.50462.0001). The column was maintained at 40°C, and the injection volume of all samples was 2 μL. The mobile phase A consisted of 15 mM ammonium acetate and 3 ml/L Ammonium Hydroxide (> 28 %) in LC-MS grade water. The mobile phase B consisted of LC−MS grade 90 % (v/v) acetonitrile in HPLC water. The mobile phase ran at a flow rate of 0.2 mL/min, and the column was eluted with the following gradient program: 95% B held for 2 min, increased to 45 % B in 13 min, held for 3 min, and the post time was set for 4 min. The QTRAP mass spectrometer used a Turbo V ion source. The ion source was run in negative mode with a spray voltage of -4,500 V, Gas1 40 psi and Gas2 50 psi and Curtain gas 35 psi. Metabolites were measured using the multiple reactions monitoring mode (MRM), and the relative amounts of metabolites were analyzed by MultiQuant Software (AB SCIEX).

Ly6G depletion assay

To perform the Ly6G antibody depletion assay, mice were first injected with IL-4c as previously described. Three hours later, the mice were injected with either 150 μg of anti-mouse Ly6G antibody (BioXCell, 1A8) or IgG2a isotype control (BioXCell, 2A3) diluted in 200 μL of PBS. After 18 hours, blood was collected to determine the efficiency of Ly6G antibody depletion.

Western blot

Cells were lysed with RIPA buffer (1 mM Tris-HCl, 0.3 M NaCl, 0.01% SDS, 1.5% NP40, 120 mM deoxycholate, 1 M MgCl2) containing protease inhibitors. The proteins were resolved by SDS-PAGE and transferred to PVDF membranes (catalog number Roche, # 3010040001). The membranes were then blocked for 1 hour in blocking buffer (5% BSA and 0.1% Tween 20 in TBS) at room temperature, and incubated with respective primary antibodies in 5% BSA containing TBST at 4°C overnight. The membranes were then washed and subjected to HRP-coupled secondary antibodies in TBST at room temperature for 1 hour. Antibodies against β-Actin (catalog number 21338) and pfkfb3 (catalog number 49656) were purchased from SAB. Antibodies against HK1 (catalog number A10886), HK3 (catalog number A8428), Glut1 (catalog number A11727), Histone H3 (catalog number A2348), Hif1α (catalog number A11945), and Wdr5 (catalog number A2023) were purchased from ABclonal. Antibodies against Aldolase A (catalog number 8086), Enolase-1 (catalog number 3810), Stat6 (catalog number 5397), and Tri-Methyl-Histone H3 (Lys4) (catalog number 9751) were purchased from CST. The antibody against IL-1 beta (catalog number ab234437) was purchased from Abcam.

RNA-seq data analysis

To analyze the RNA-seq data, the paired-end sequence reads were aligned to the mouse genome reference (mm10) with HISAT2 using the default options. The reads that mapped to each gene were named "raw-count" through feature-count, and the FPKM of each gene was calculated based on the length of the gene and its raw count. The differential gene expression analysis was performed using DESeq2, and the differentially expressed genes were selected based on their fold change and significance relative to two biological replications. Only genes with a fold change above 2 and p-values below 0.05 were considered significant. The pathway analysis was performed using ClusterProfiler (R), with the resulting p-value cut off at 0.05. All heatmaps were created using ComplexHeatmap in R. The RNAseq data have been deposited in the GEO database with accession number GSE184811.

CUT&Tag-seq and ATAC-seq data analysis

The CUT&Tag-seq and ATAC-seq data were analyzed as follows. First, the paired-end reads were aligned to the mouse reference genome (mm10) using bowtie2 with the default options. The resulting aligned reads were converted to a sorted BAM format using samtools. Peaks were called using MACS2 with a q-value threshold of 0.05, model fold ranging from 5-50, and the "keep-dup all" option to keep all tags. Bedtools was used to count the peaks, and the counts were normalized to reads per kilobase per million mapped reads (RPKM). The resulting peaks were annotated using the ChIPseeker package, and pathway analysis was performed using the ClusterProfiler package. GSEA analysis was conducted using the msigdb_v2022.1.Mm database. The data have been deposited in the GEO database with accession number GSE196099.

QUANTIFICATION AND STATISTICAL ANALYSIS

Differences between groups were analyzed using the two-tailed Student's t-test. The results were reported as means ± standard deviation (SD), and statistical significance was indicated by a p-value less than 0.05, denoted by a star symbol (*). The Prism software (GraphPad) was used for all statistical analyses.